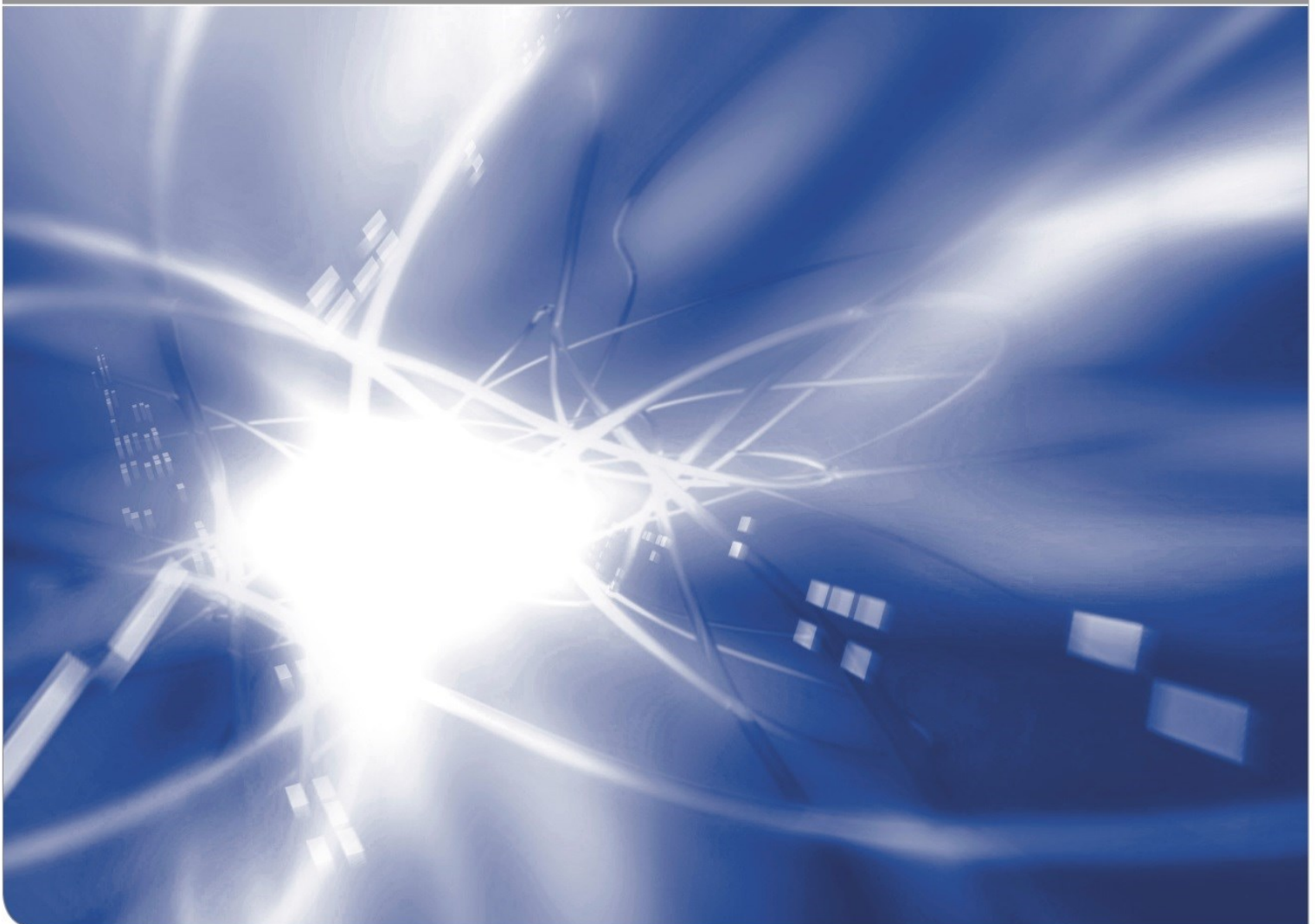


Uncertainties of displacement cross-sections for iron and tungsten at neutron irradiation energies above 0.1 MeV

by A.Yu. Konobeyev, U. Fischer, S.P. Simakov

KIT SCIENTIFIC WORKING PAPERS 49



Institute for Neutron Physics and Reactor Technology, KIT

Impressum

Karlsruher Institut für Technologie (KIT)
www.kit.edu



Diese Veröffentlichung ist im Internet unter folgender Creative Commons-Lizenz
publiziert: <http://creativecommons.org/licenses/by-nc-nd/3.0/de>

2016

ISSN: 2194-1629

KIT Scientific Working Papers
ISSN 2194-1629

www.kit.edu

Abstract

Uncertainty of atomic displacement cross-sections was estimated for iron and tungsten irradiated with neutrons of intermediate energy. The TALYS and ECIS codes were applied for recoil energy distribution calculations in the energy range 0.1 to 150 MeV; the CASCADE code implementing the intranuclear cascade evaporation model was used at the energies from 100 MeV to 3 GeV.

The NRT model and the arc-dpa approach were applied for calculation of the number of stable defects produced under irradiation.

CONTENTS

	page
1. Introduction	1
2. Incident neutron energies from 0.1 to 150 MeV	3
2.1 Iron	3
2.1.1 Components of displacement cross-section	5
2.1.1.1 Neutron elastic scattering	6
2.1.1.2 Neutron inelastic discrete-level scattering	8
2.1.1.3 Reactions	9
2.1.2 Total displacement cross-section	10
2.2 Tungsten.....	13
3. Incident neutron energies up to 3 GeV	16
3.1 Difference in displacement cross-section calculated using different models	16
3.2 Uncertainty of displacement cross-sections obtained from the variation of parameters of intranuclear cascade evaporation model	17
4. Conclusion	18
References	19
Appendix A: Results of ECIS code calculations for iron using the Koning-Delaroche optical potential	21
Appendix B: The RSD values of elastic scattering component of displacement cross-section for iron	27
Appendix C: The RSD values of inelastic discrete-level scattering component of displacement cross-section for iron	30
Appendix D: Examples of RSD values of cross-sections and displacement cross-sections for (n,np) and (n,3n) reactions for iron	33
Appendix E: The RSD values of elastic scattering, inelastic discrete-level scattering, (n,2n), (n,np), and (n,3n) reaction components of displacement cross-section for tungsten	35

1. Introduction

The goal of the work is the evaluation of uncertainties of calculated atomic displacement cross-sections for iron and tungsten irradiated with neutrons. Uncertainties were analysed for neutron incident energies above 0.1 MeV making the main contribution to the value of radiation damage rate calculated for different types of nuclear and fusion reactors, and neutron sources [1].

Covariance matrices for displacement cross-section (σ_d) and its components were calculated using the Monte Carlo method proposed in Ref.[2]. The procedure consists of i) the choice of the basic set of model parameters, ii) the estimation of the standard deviation of model parameters, iii) the Monte Carlo sampling of the N number of input data sets, iv) the execution of calculations for obtained N input data files, and v) the processing of results and the computation of covariance matrices

$$V_{ij} = N^{-1} \sum_{k=1}^N (\sigma_{d,ik} - \sigma_{d,i0}) (\sigma_{d,jk} - \sigma_{d,j0}) \quad (1)$$

where $\sigma_{d,ik}$ is the displacement cross-section corresponding to the “i”-th primary neutron energy in the “k”-th Monte Carlo event, $\sigma_{d,i0}$ is the cross-section calculated using set of unchanged model parameters.

The corresponding correlation matrix is calculated as follows

$$C_{ij} = V_{ij} / \sqrt{V_{ii} \times V_{jj}} \quad (2)$$

and the standard deviation of displacement cross-section is equal to

$$\Delta\sigma_{d,ii} = \sqrt{V_{ii}} \quad (3)$$

Recoil energy distributions were calculated for different input data sets using the TALYS-1.8 code [3] at incident neutron energies from 0.1 to 150 MeV and the CASCADE-2014 code [4,5] at neutron energies from 100 MeV to 3 GeV.

The uncertainties of displacement cross-section were estimated using both the NRT model [6] and the arc-dpa approach [7,8].

When using the NRT model four parameters were varied. Three parameters relate to the numerical coefficients in $g(\epsilon)$ formula [6] obtained in Ref.[9] by approximating the Lindhard's function:

$$g(\epsilon) = 3.4008 \epsilon^{1/6} + 0.40244 \epsilon^{3/4} + \epsilon, \quad (4)$$

the fourth parameter is the effective threshold displacement energy E_d .

According to the “athermal recombination corrected dpa” (arc-dpa) concept the number of stable defects produced under irradiation is calculated as follows [7,8]

$$N_d(T_{dam}) = \begin{cases} 0 & \text{when } T_{dam} < E_d \\ 1 & \text{when } E_d < T_{dam} < 2E_d / 0.8 \\ \frac{0.8}{2E_d} \xi_{arc dpa}(T_{dam}) T_{dam} & \text{when } 2E_d / 0.8 < T_{dam} \end{cases}, \quad (5)$$

where T_{dam} is the “damage energy” i.e. the energy available to produce displacement by elastic collisions [6] calculated using the Robinson formula [10]. The defect generation efficiency is equal to [7,8]

$$\xi_{arc dpa}(T_{dam}) = \frac{1 - c_{arc dpa}}{(2E_d / 0.8)^{b_{arc dpa}}} T_{dam}^{b_{arc dpa}} + c_{arc dpa} \quad (6)$$

The arc-dpa parameters obtained in Ref.[8] by fitting of results of molecular dynamics simulations are given in Table 1.

Two parameters $b_{arc dpa}$ and $c_{arc dpa}$, Eq.(6) were varied when using the arc-dpa approach for iron and tungsten. In this case the NRT parameters in Eq.(5) and the E_d value, i.e. the T_{dam} values remained unchanged.

The variation of parameters of nuclear models and defect production models was done using a normal distribution. The Δp -value shown in figures and discussed below is the relative standard deviation (RSD) or the coefficient of variation (CV) concerning the σ/μ ratio of the normal distribution.

Table 1. Fitting parameters of the arc-dpa for Fe and W [8].

Material	E_d	$b_{arc dpa}$	$c_{arc dpa}$
Fe	40	-0.568 ± 0.020	0.286 ± 0.005
W	70	-0.564 ± 0.018	0.119 ± 0.005

The MC variation of NRT model parameters is controversial. Model predictions differ from available experimental data and results of MD modelling. It seems impractical to compensate the shortcomings of the model by large uncertainty of model parameters. NRT may be used for the comparison of radiation damage rates in different units and not for prediction of real number of stable defects produced under the irradiation.

The argument for the variation of model parameters relates to the fact that NRT-parameters are directly related to experimental data and therefore have an error. In addition, it is reasonable to compare different damage rates calculated in terms of “NRT-dpa” with estimated errors.

2. Incident neutron energies from 0.1 to 150 MeV

Energy and angular particle distributions, and recoil spectra were calculated using the TALYS-1.8 code [3]. Optical model calculations were performed with the Koning-Delaroche potential [11].

The calculations for iron were made using TALYS with 6,700 MC-generated input data files, for tungsten with 3,200 input data files.

The recoil spectra for neutron elastic and inelastic discrete-level scattering (n,n') were obtained using calculated neutron angular distribution. A special procedure was applied to get recoil spectra for neutron inelastic continuum scattering using results of TALYS-1.8 calculations. All calculations discussed below were performed with the variation of nuclear level density parameters with RSD value $\Delta\rho(\text{levd})$ equal to 10 %.

The uncertainty of shape elastic scattering contribution in displacement cross-section was estimated using the ECIS code [12].

2.1 Iron

Fig.1 shows an example of the number of defects calculated with varied NRT and arc-dpa parameters with RSD values $\Delta\rho$ equal to 20%. The effective threshold displacement energy E_d is equal 40 MeV.

Fig.2 shows the arc-dpa defect production efficiency calculated with $\Delta\rho$ equal to 20% and the approximation [7,8] of results of MD simulations.

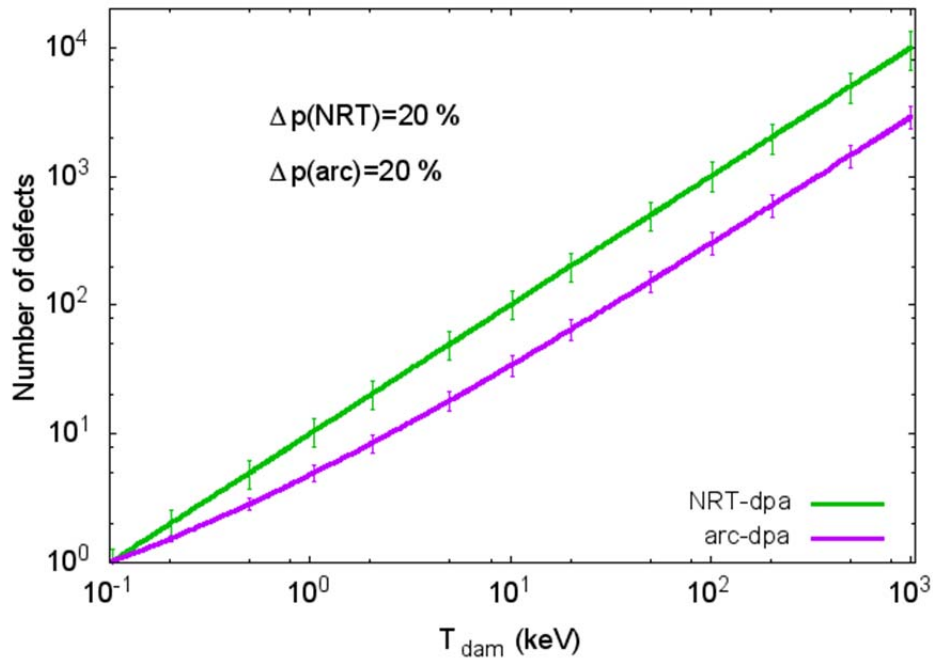


Fig.1 The number of defects calculated for iron using the NRT model and the arc-dpa approach with the coefficient of variation of NRT and arc-dpa parameters equal to 20%.

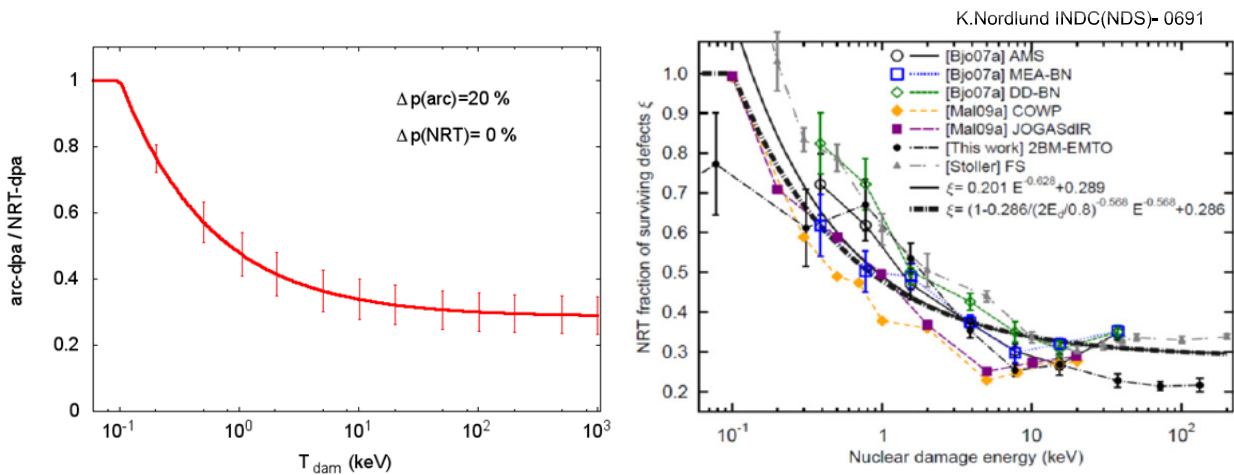


Fig.2 The efficiency of defect generation calculated with the coefficient of variation of arc-dpa parameters equal to 20% (left) and the same values (thick dash-dot line) compared with results of different MD simulations [8] (right) for iron.

Fig.3 shows the RSD values of the number of defects depending on different parameter variation.

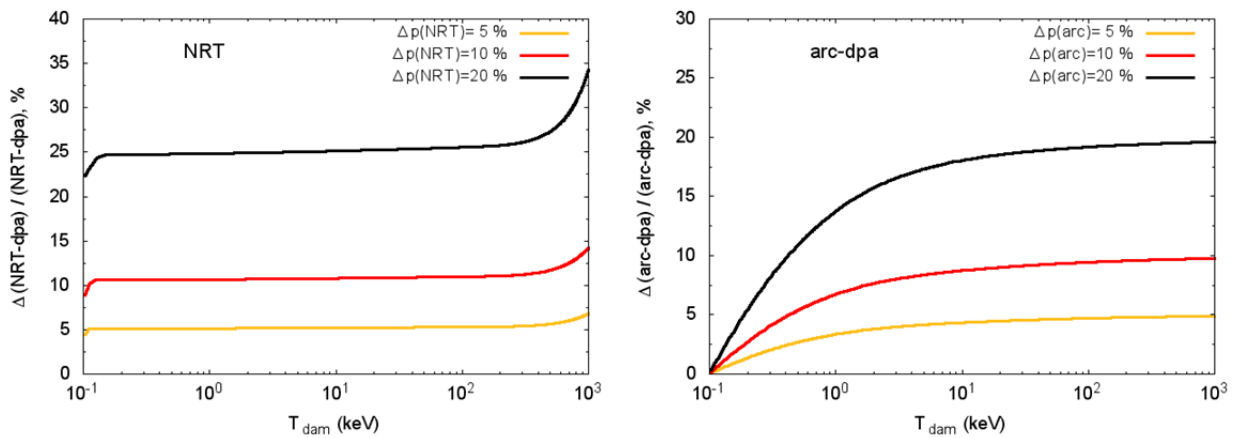


Fig.3 The RSD values of number of defects calculated using the NRT model and the arc-dpa approach with different variation of NRT and arc-dpa parameters for iron.

2.1.1 Components of displacement cross-section

Figures 4 and 5 show the contributions of elastic and nonelastic neutron interactions in the total cross-section and in the total displacement cross-section for iron. The contributions calculated using NRT and arc-dpa are similar (Fig.5).

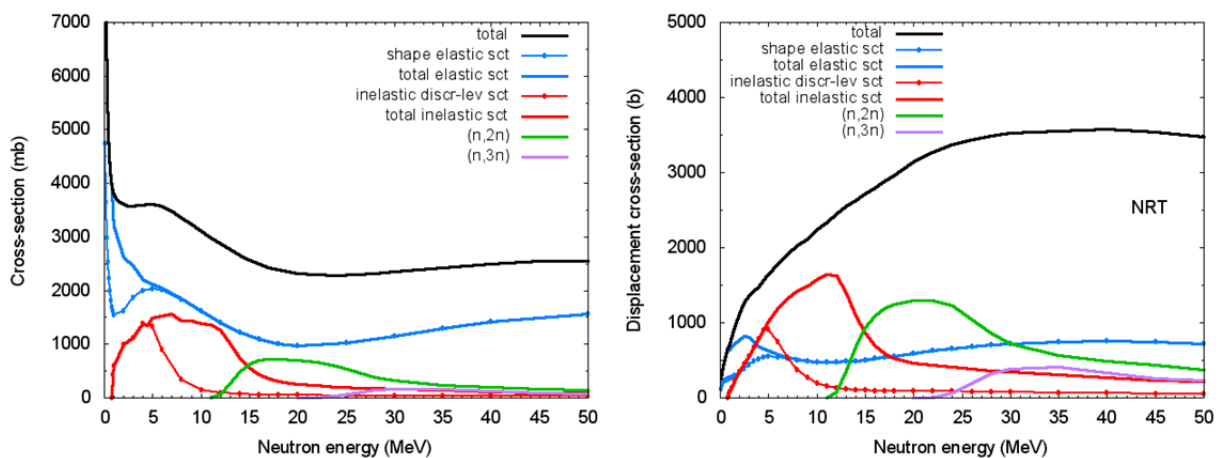


Fig.4 The total cross-section (left) and the total displacement cross-section (right) and contributions of elastic scattering and some reactions calculated using NRT at primary energies up to 50 MeV for iron.

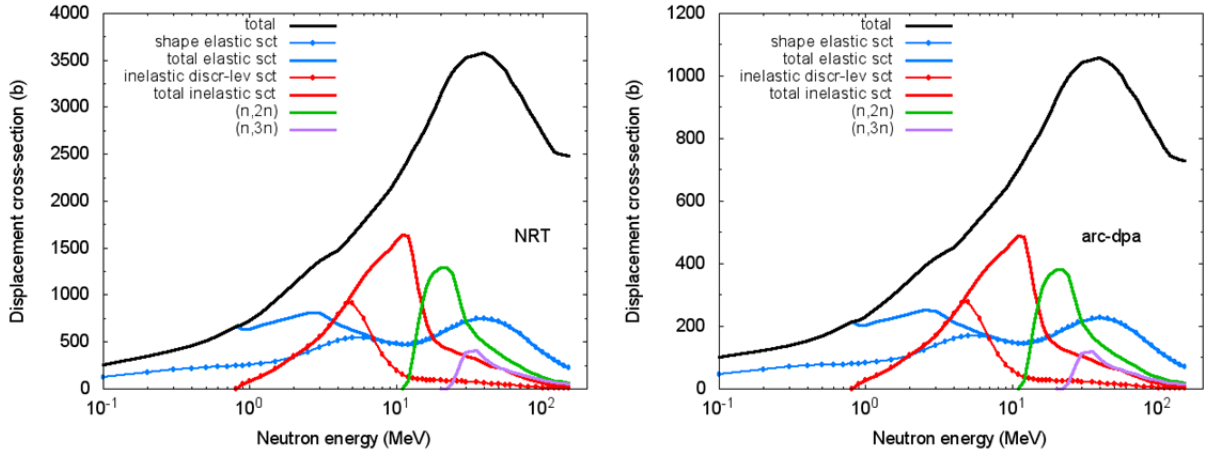


Fig.5 The total displacement cross-section calculated using NRT (left) and arc-dpa approach (right) with contributions of elastic and some nonelastic channels for iron.

2.1.1.1 Neutron elastic scattering

The uncertainty of shape elastic component of displacement cross-section was evaluated using the ECIS code [12].

Calculations with ECIS were performed for two types of variation of optical model parameters [11]. In the first set of calculations, the V , W , and W_d parameters of the optical potential [3] values were varied, in the second set all input variable of ECIS were modified. The number of MC-generated input files is 5,000 for the first type of calculations and 20,000 for the second type. The results are shown in Appendix A.

The first type of variation was applied in all TAYLS calculations discussed below.

The contribution of neutron elastic scattering (shape elastic and compound parts) in the displacement cross-section was calculated using the TALYS code.

Fig.6 shows the RSD of elastic scattering cross-section for iron calculated with different variation of optical model parameters and TENDL-2015 data [13]. Fig.7 shows $\Delta\sigma_{d,el}/\sigma_{d,el}$ values calculated using the NRT model and arc-dpa approach with different variation of NRT and arc-dpa parameters and variation of optical model parameters with the RSD value $\Delta p(\text{opt})$ equal to 5%.

The results obtained with other variation of optical model parameters and with different variation of NRT and arc-dpa parameters are shown in Appendix B.

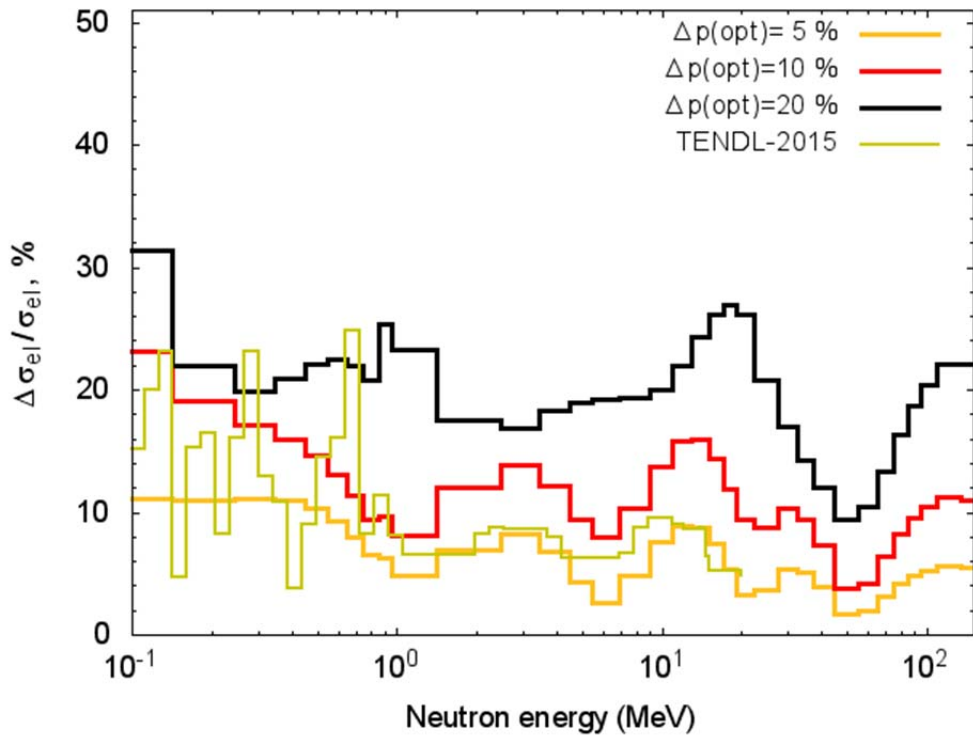


Fig.6 The RSD values of elastic scattering (shape elastic and compound) cross-section for iron calculated with different variation of optical model parameters and TENDL-2015 data. See details in the text.

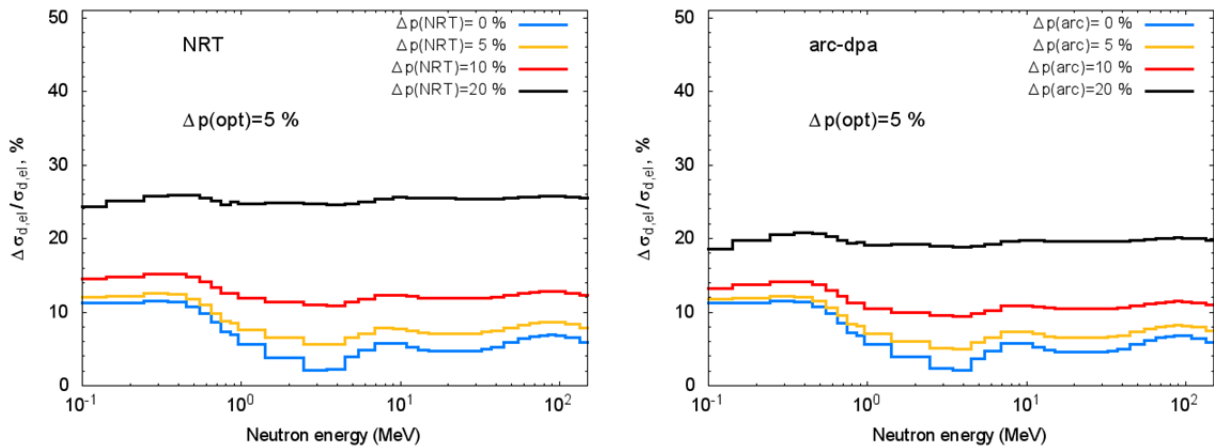


Fig.7 The RSD values of elastic scattering (shape elastic and compound) component of displacement cross-section for iron calculated using the NRT model (left) and the arc-dpa approach (right) with different variation of NRT and arc-dpa parameters and variation of optical model parameters with the RSD value $\Delta p(\text{opt})$ equal to 5%.

2.1.1.2 Neutron inelastic discrete-level scattering

Fig.8 shows the RSD values of inelastic discrete-level scattering cross-section for iron calculated using TALYS-1.8 with different variation of optical model parameters and TENDL-2015 [13] data for sum of inelastic discrete-level and inelastic continuum scattering.

Fig.9 shows RSD values of the component of displacement cross-section concerning neutron inelastic discrete-level scattering obtained with different variation of NRT and arc-dpa parameters and variation of optical model parameters with RSD equal to 5 %.

The results of calculations with different variation of optical model, NRT, and arc-dpa parameters are given in Appendix C.

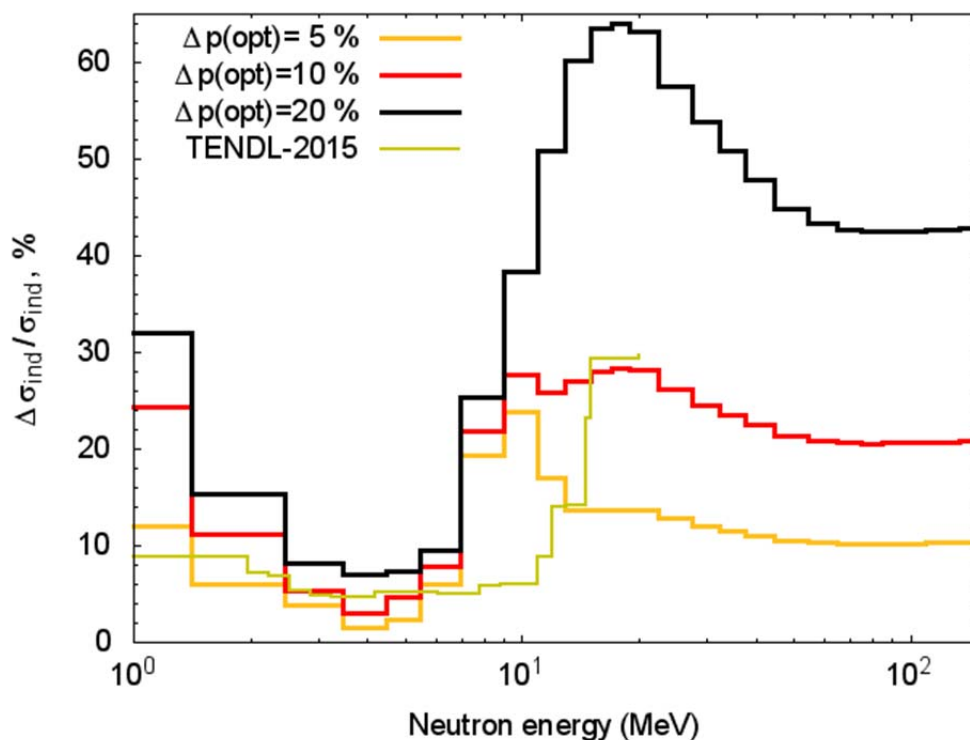


Fig.8 The RSD values of inelastic discrete-level scattering cross-section for iron calculated using TALYS-1.8 with different variation of optical model parameters and TENDL-2015 data*.

* Data from TENDL-2015 [13] correspond to MT=4 section of the ENDF/B formatted file

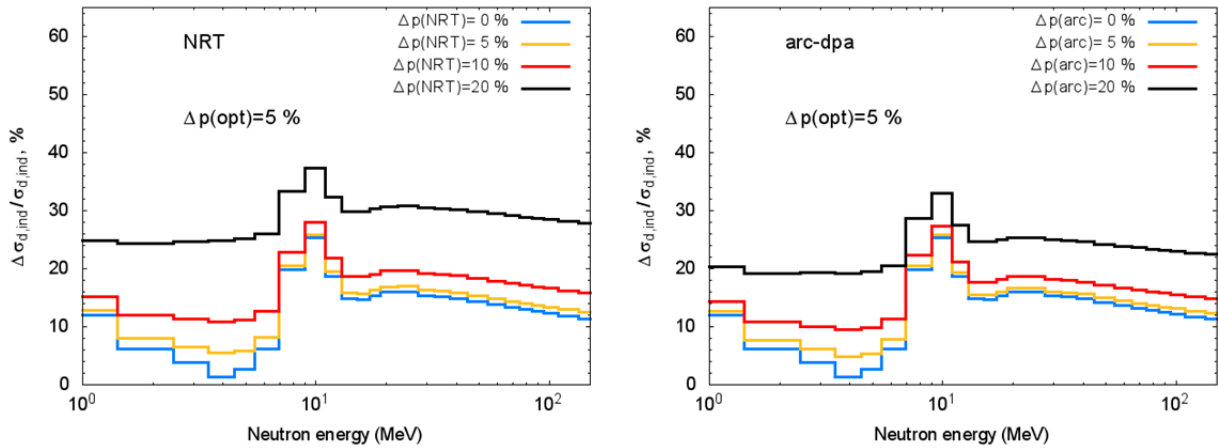


Fig.9 The RSD values of inelastic discrete-level scattering component of displacement cross-section for iron calculated with TALYS-1.8 using the NRT model (left) and the arc-dpa approach (right) with different variation of NRT and arc-dpa parameters and variation of optical model parameters with the RSD value $\Delta p(\text{opt})$ equal to 5%.

2.1.1.3 Reactions

Figures 10 and 11 show the example of RSD of (n,2n) reaction cross-section and corresponding component of displacement cross-section. The $\Delta\sigma_{(n,2n)}/\sigma_{(n,2n)}$ values for cross-sections are shown in Fig.10 together with TENDL-2015 data [13]. The variation of optical model and nuclear level density parameters was performed with adopted RSD values of parameters equal to 5% and 10%, correspondingly.

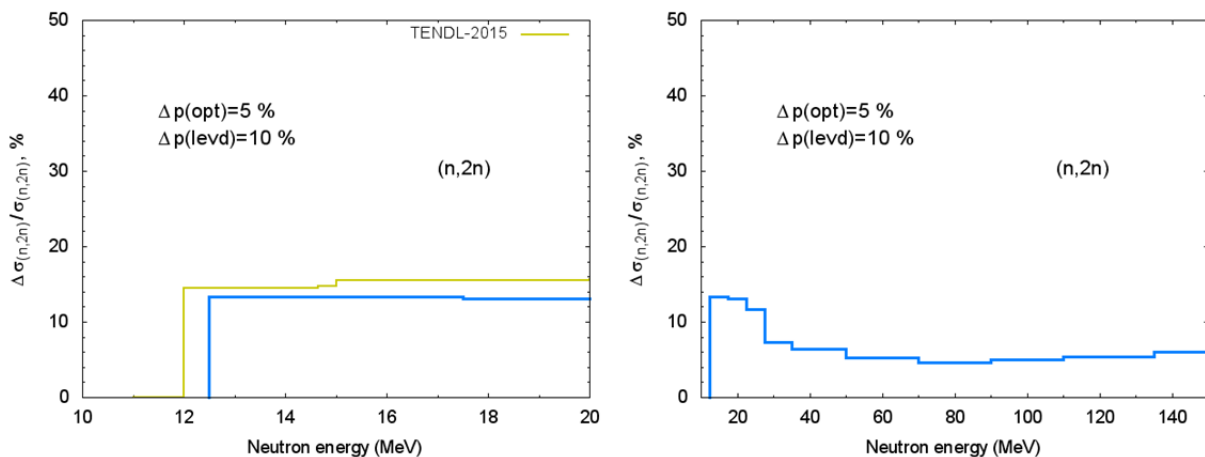


Fig.10 The calculated RSD values of (n,2n) reaction cross-section for iron and TENDL-2015 data (left). See details in the text.

Fig.11 presents the results obtained for (n,2n) components of displacement cross-section. Examples for other reactions can be found in Appendix D.

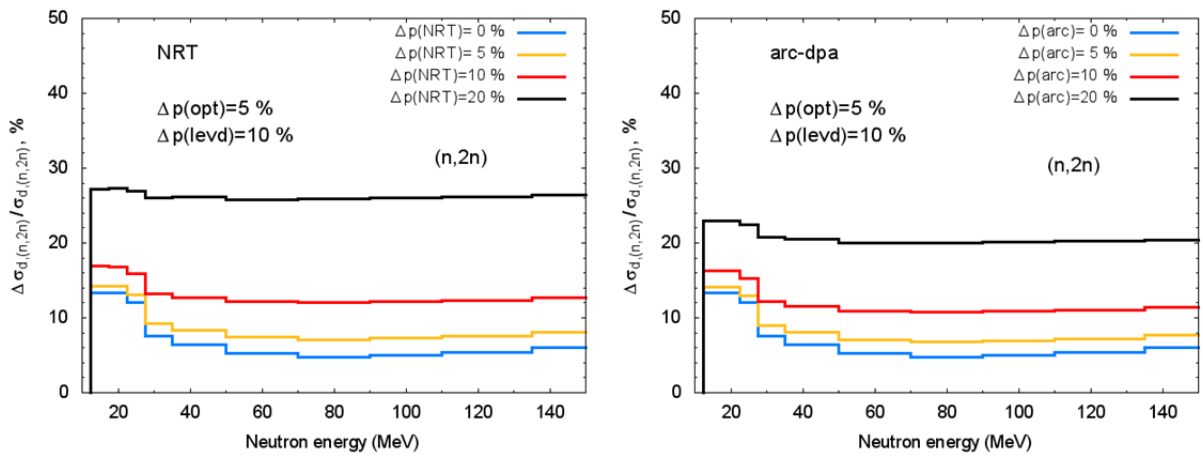


Fig.11 The RSD values of (n,2n) reaction component of displacement cross-section for iron calculated using the NRT model (left) and the arc-dpa approach (right) with different variation of NRT and arc-dpa parameters, and the variation of optical model and nuclear level density parameters with the RSD values equal to 5% and 10%, correspondingly.

2.1.2 Total displacement cross-section

Fig.12 shows RSD values of the total cross-section calculated with different variation of optical model parameters, TENDL-2015 data [13], and the example of calculated total, elastic scattering (shape elastic and compound), inelastic discrete-level scattering, and (n,2n) cross-sections with errors corresponding to the variation of optical model and nuclear level density parameters with RSD equal to 5% and 10% respectively.

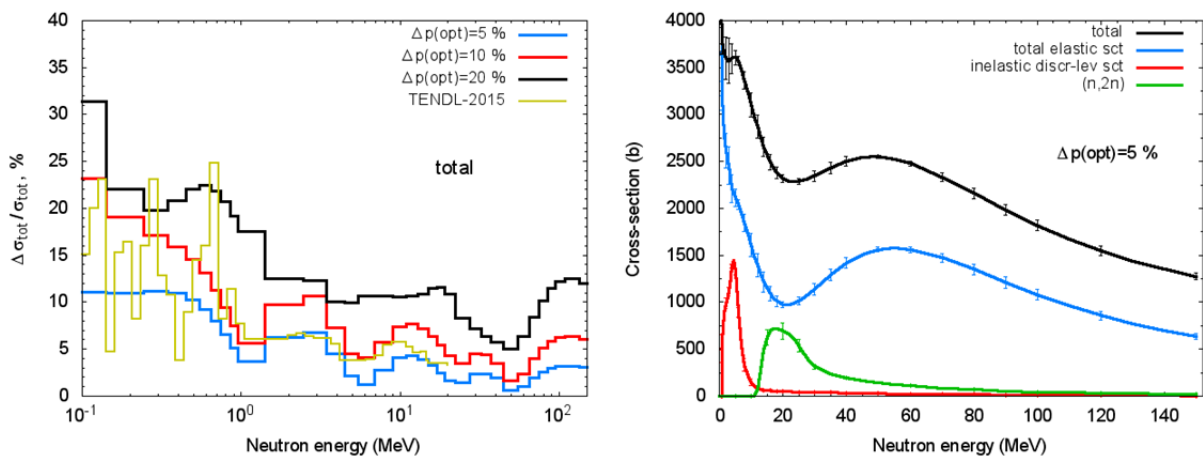


Fig.12 The calculated RSD values of total cross-section and TENDL-2015 data (left), and the example of calculated total cross-section and its several components with errors (right) for iron. See explanations in the text.

Fig.13 shows the example of the total displacement cross-section (sum of components for all neutron channels) with errors calculated using the NRT model and the arc-dpa approach with the variation of NRT, and arc-dpa parameters with RSD values equal to 10%. Some components of total displacement cross-section: are also shown.

The RSD values of total displacement cross-section obtained with different variation of NRT and arc-dpa parameters are shown in Fig.14.

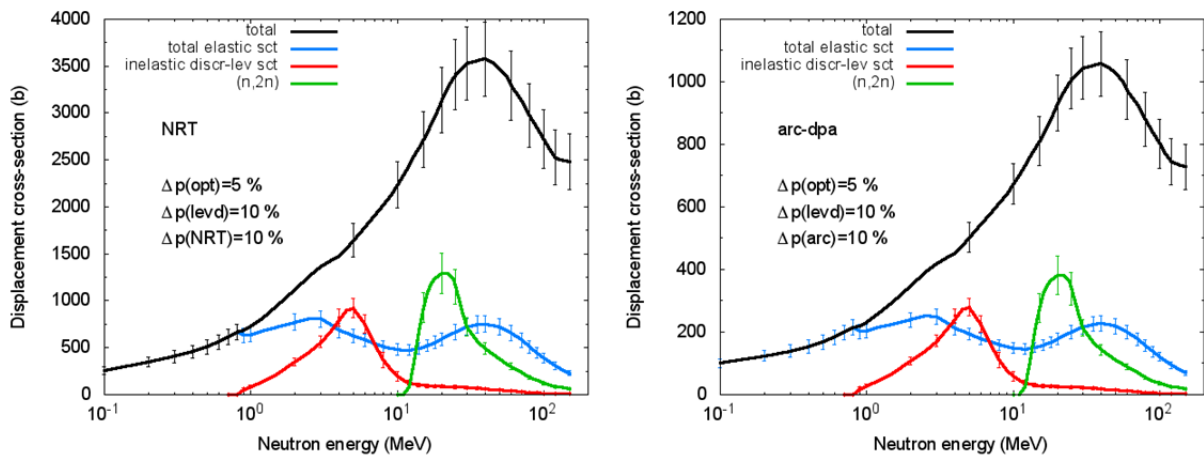


Fig.13 The total displacement cross-section and some its components calculated for iron using the NRT model (left) and the arc-dpa approach (right) with errors corresponding to the variation of optical model parameters, nuclear level density parameters, NRT, and arc-dpa parameters with RSD values equal to 5%, 10%, 10%, and 10%, correspondingly.

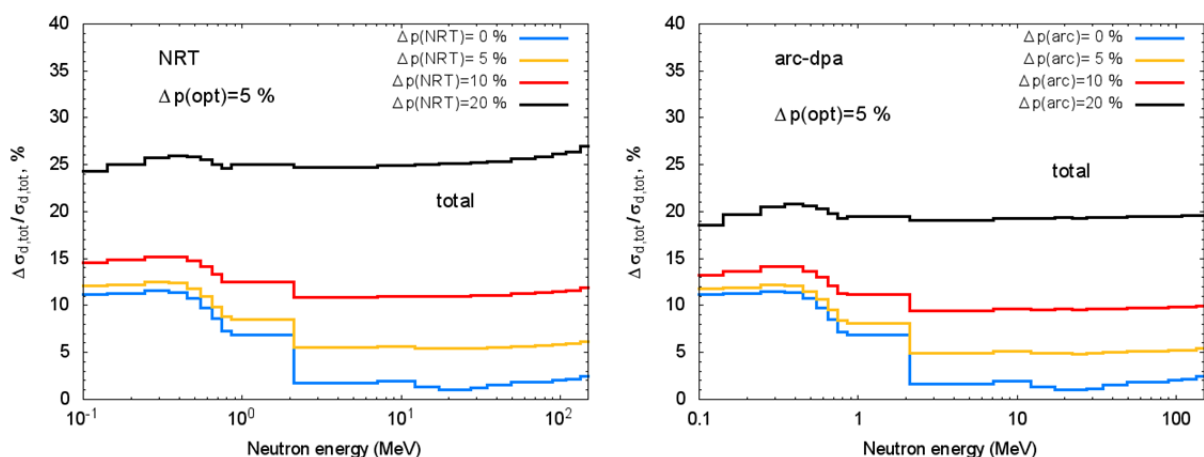


Fig.14 The RSD values of total displacement cross-section calculated for iron using the NRT model (left) and the arc-dpa approach (right) with different variation of NRT and arc-dpa parameters, and the variation of optical model and nuclear level density parameters with the RSD values equal to 5% and 10%, correspondingly.

Fig.15 presents the example of the correlation matrix for the total displacement cross-section calculated using the NRT model without variation of NRT parameters and with the RSD value $\Delta p(\text{NRT})$ equal to 5 %. The RSD values of nuclear model parameters are discussed above in this Section. The figure illustrates an appearance of strong correlations after taking into account the variation of parameters of defect production models.

The correlations obtained using the NRT and arc-dpa model are compared in Fig.16. The only difference between Fig.15 (right) and Fig.16 (left) is the different scale.

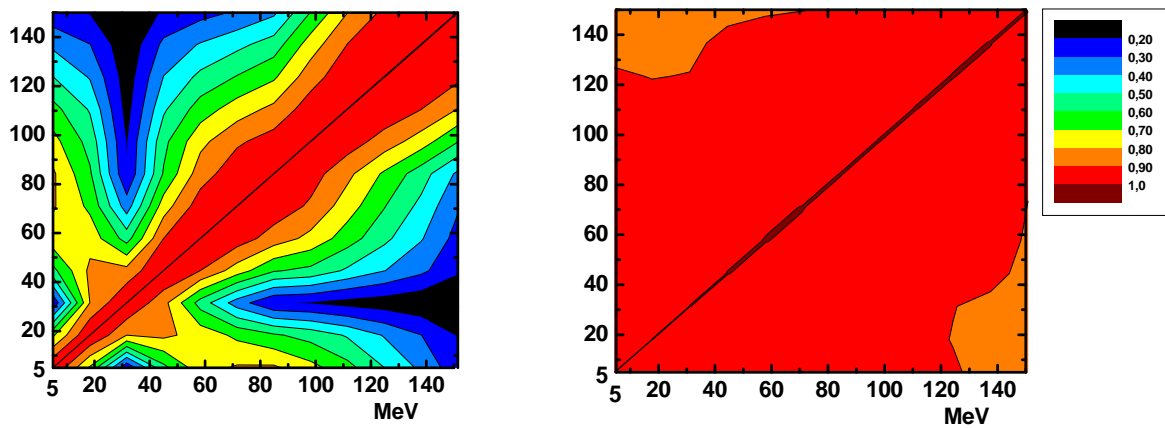


Fig.15 The correlation matrices for total displacement cross-section for iron calculated using the NRT model without the variation of NRT parameters (left) and with the variation of parameters with RSD value $\Delta p(\text{NRT})$ equal to 5 %. See explanations in the text.

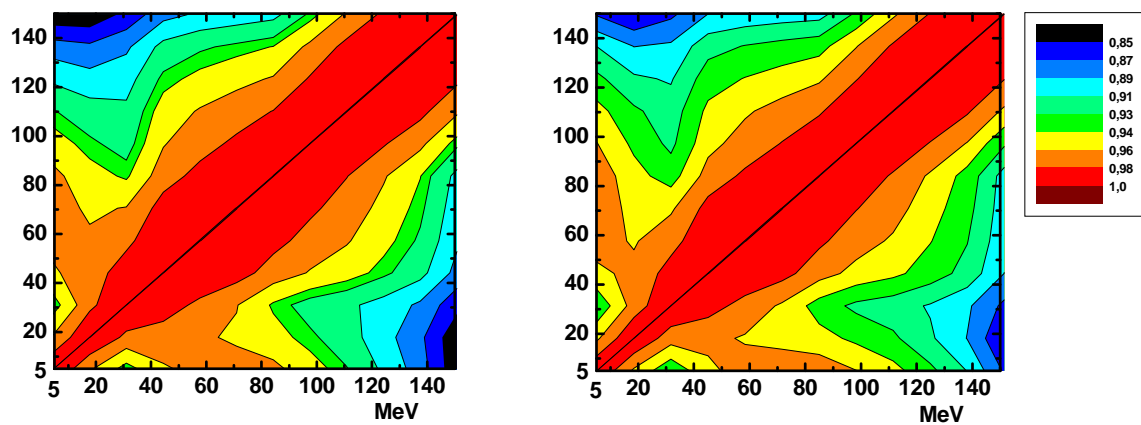


Fig.16 The correlation matrices for total displacement cross-section for iron calculated using the NRT model (left) and the arc-dpa approach (right) with the $\Delta p(\text{NRT})$ and $\Delta p(\text{arc})$ values equal to 5 %. See explanations in the text.

2.2 Tungsten

Fig.17 shows the example of the number of defects and defect generation efficiency with errors calculated by variation of NRT and arc-dpa parameters with the RSD values equal to 20%. The effective threshold displacement energy E_d is equal 70 MeV (Table 1, Ref.[8]).

Fig.18 shows the RSD values of the number of defects obtained with different variation of NRT and arc-dpa parameters.

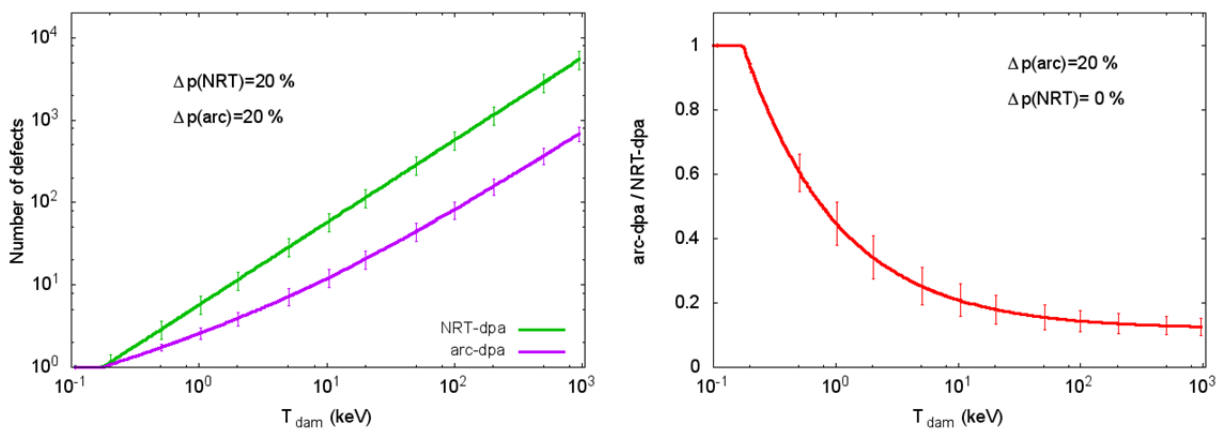


Fig.17 The number of defects calculated for tungsten using the NRT model and the arc-dpa approach (left) and the efficiency of defect generation (right) calculated for tungsten with the coefficient of variation of NRT and arc-dpa parameters equal to 20%. The E_d value is equal to 70 eV [8].

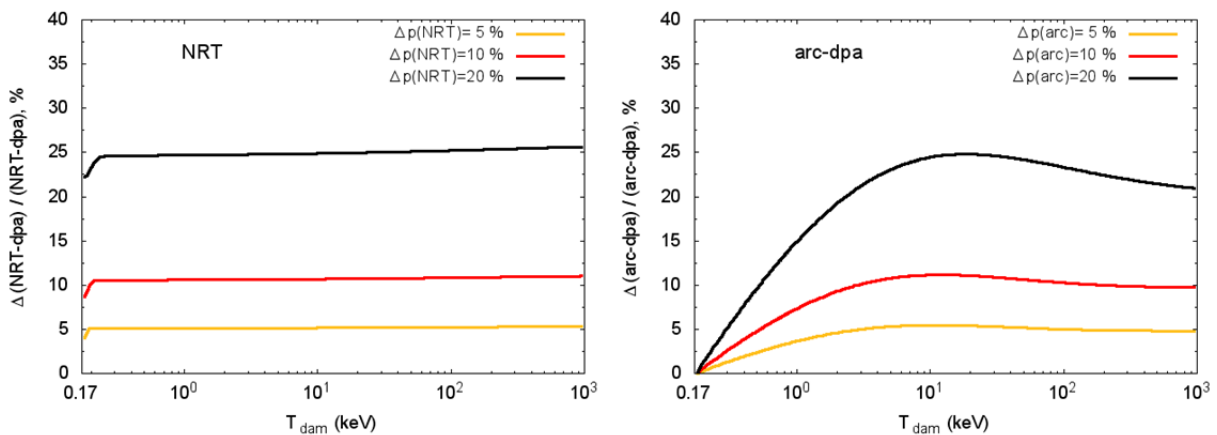


Fig.18 The RSD values of number of defects calculated using the NRT model (left) and the arc-dpa approach (right) for tungsten.

Results obtained for the total cross-section and the total displacement cross-section are discussed below. Other information about the components of displacement cross-sections can be found in Appendix E.

Fig.19 shows RSD values of the total cross-section for tungsten calculated with different variation of optical model parameters, TENDL-2015 data [13], and the example of calculated cross-sections for various channel with errors corresponding to the variation of optical model parameters with RSD value equal to 5 %, and nuclear level density parameters with RSD equal to 10%.

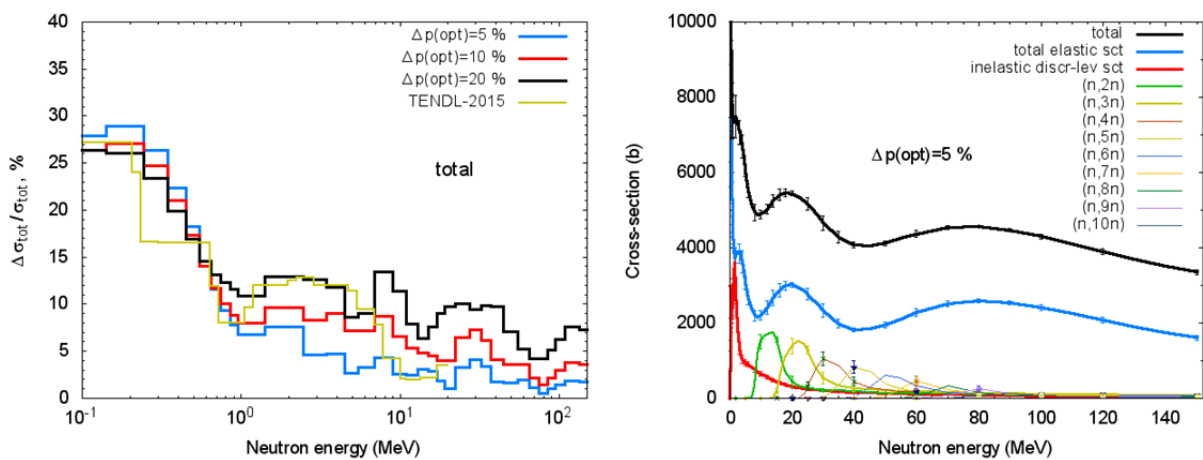


Fig.19 The calculated RSD values of total cross-section and TENDL-2015 data for tungsten (left); the example of calculated total cross-section, elastic scattering cross-section, inelastic discrete-level scattering cross-section, and some (n,xn) reaction cross-sections with errors for tungsten (right). See explanations in the text.

Fig.20 shows the example of the total displacement cross-section, elastic scattering cross-section, inelastic discrete-level scattering cross-section, and (n,xn) reaction cross-sections with errors calculated using the NRT model and the arc-dpa approach with the variation of NRT, and arc-dpa parameters with RSD values equal to 10%.

The RSD values of total displacement cross-section for tungsten obtained with different variation of NRT and arc-dpa parameters are shown in Fig.21.

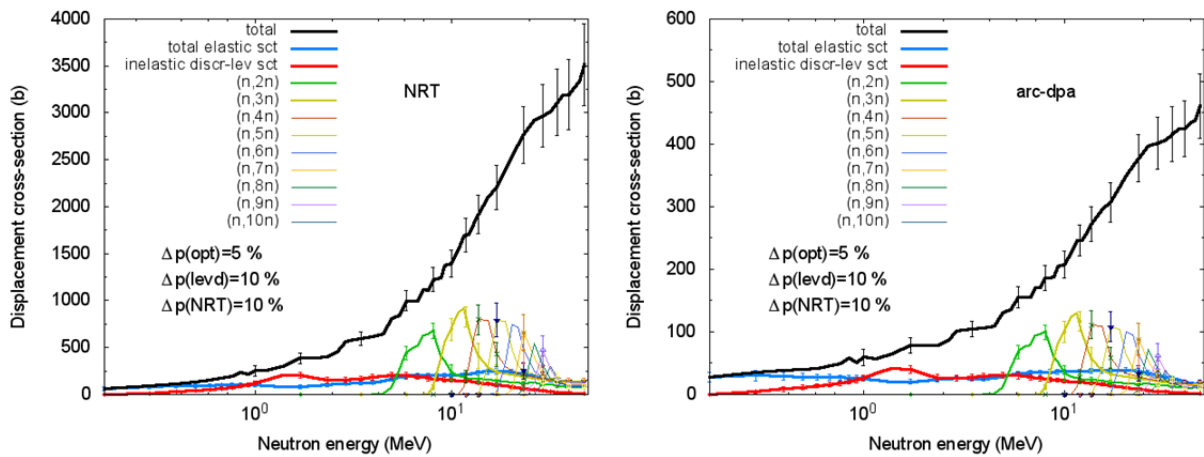


Fig.20 The total displacement cross-section and some its components for tungsten calculated using the NRT model (left) and the arc-dpa approach (right) with errors relating to the variation of following parameters and corresponding RSD values: optical model parameters (5%), nuclear level density parameters (10%), NRT parameters (10%), and arc-dpa parameters (10%). The E_d value is equal to 70 eV [8].

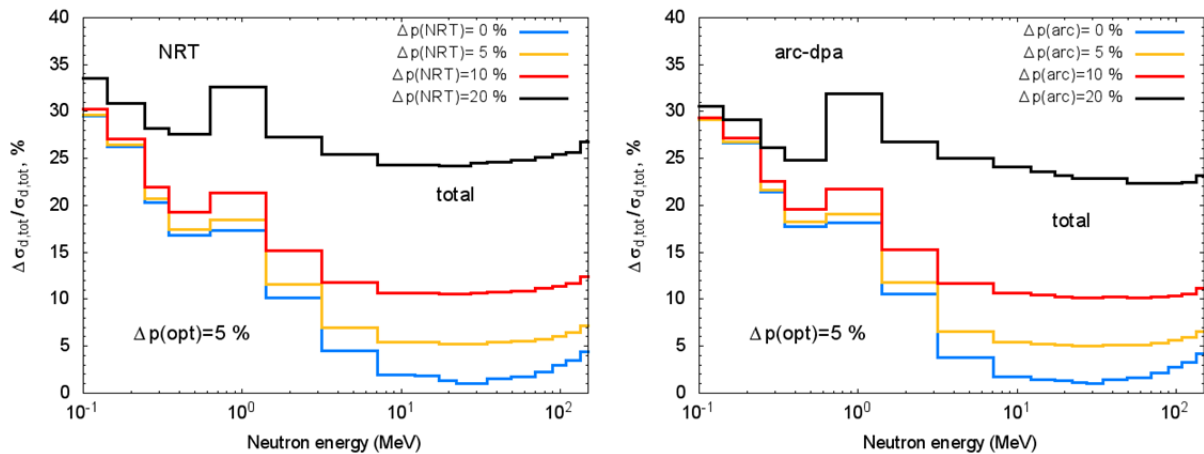


Fig.21 The RSD values of total displacement cross-section for tungsten calculated using the NRT model (left) and the arc-dpa approach (right) with different variation of NRT and arc-dpa parameters, and the variation of optical model and nuclear level density parameters with the RSD values equal to 5% and 10%, correspondingly.

3. Incident neutron energies up to 3 GeV

3.1 Difference in displacement cross-section calculated using different models

The calculation of displacement cross-sections was performed using different versions of the intranuclear cascade evaporation model implemented in the CASCADE code [4,5], DISCA-C code [14], and the MCNPX code [15]: Bertini/Dresner, Bertini/ABLA, ISABEL/Dresner, ISABEL/ABLA, INCL4/Dresner, INCL4/ABLA, and CEM03 models. The number of defects produced by PKA's was obtained using the NRT model [6,10] and BCA-MD approach [16,17]. The parameters of the models were not varied in this calculation.

The results are shown in Figs.22 and 23. Here the E_d value for tungsten is equal to 90 eV. Figures show that the RSD of displacement cross-section for nonelastic neutron interaction increases with the energy of neutrons above 750 MeV and reaches 20-25 % at 3 GeV.

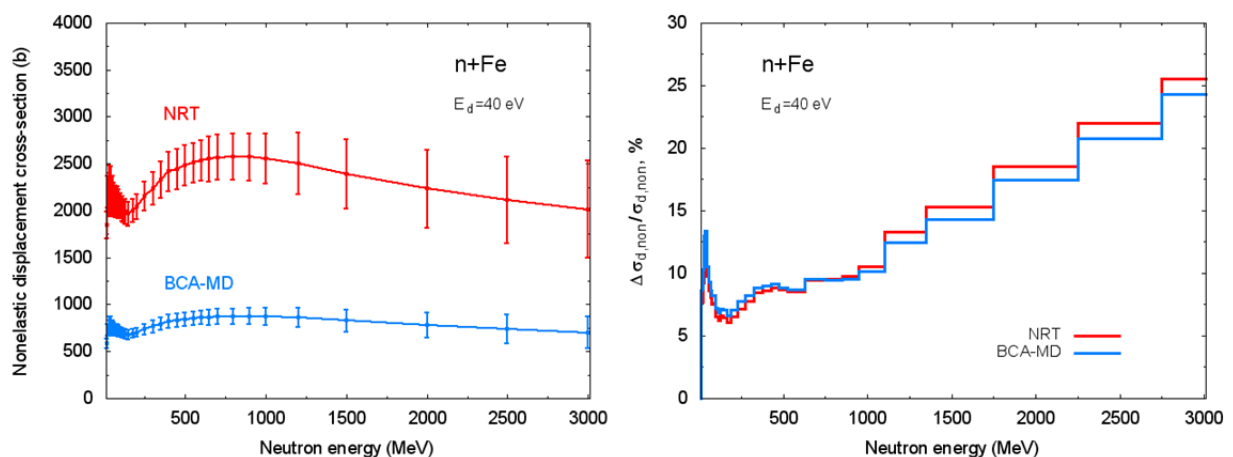


Fig.22 The displacement cross-section for nonelastic neutron interactions with iron at incident neutron energies up to 3 GeV calculated using different codes and applying the NRT model and the arc-dpa approach (left) and corresponding RSD values (right). Calculations were performed without the variation of model parameters.

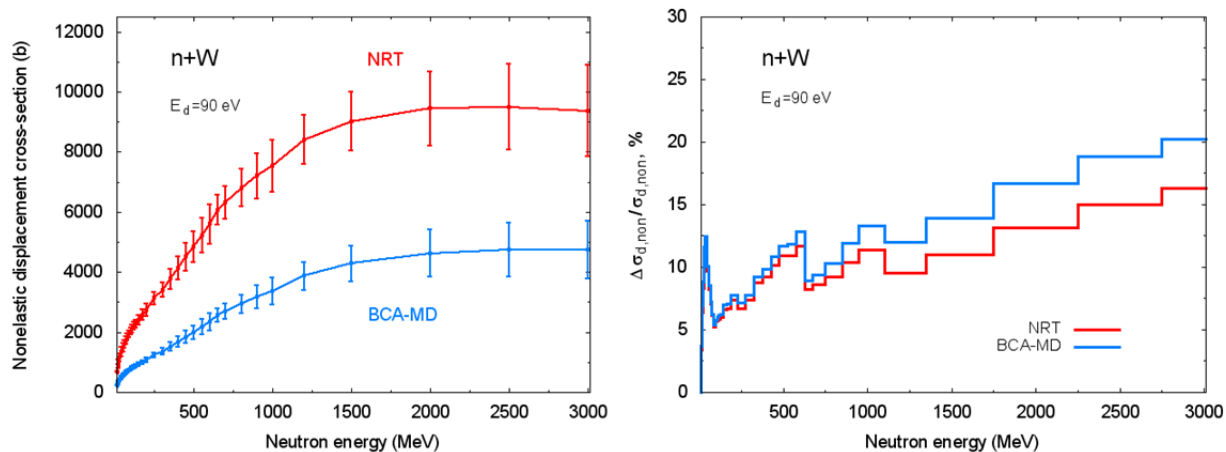


Fig.23 The displacement cross-section for nonelastic neutron interactions with tungsten at incident neutron energies up to 3 GeV calculated using different codes and applying the NRT model and the arc-dpa approach (left) and corresponding RSD values (right). Calculations were performed without the variation of model parameters. The effective threshold displacement energy E_d is equal 90 eV.

3.2 Uncertainty of displacement cross-sections obtained from the variation of parameters of intranuclear cascade evaporation model

The uncertainty of σ_d values were calculated using the CASCADE code [4,5] for iron at incident neutron energies from 100 MeV to 3 GeV with the variation of following parameters and corresponding RSD values: level density parameters (“a”) 10 %, “delta” shift of excitation energy (“ δ ”) 20 %, nucleus radius 5 %, nucleon-nucleon and nucleon-pion cross-sections 10 %, total reaction cross-section used for the normalization of results 5 %.

Obtained values are shown in Fig.24.

The comparison of results obtained at energies up to 150 MeV (Fig.14 left) and at the energy range from 100 MeV to 3 GeV (Fig.24 left) shows that the RSD of displacement cross-sections for iron obtained using different nuclear models are similar at energies from 100 to 150 MeV. At these energies nonelastic neutron interactions with nucleus make a main contribution to displacement cross-section. The closeness of results is a possible indication that the uncertainty of displacement cross-sections results mainly from the uncertainty of predictions of models for calculation of the number of stable displacements.

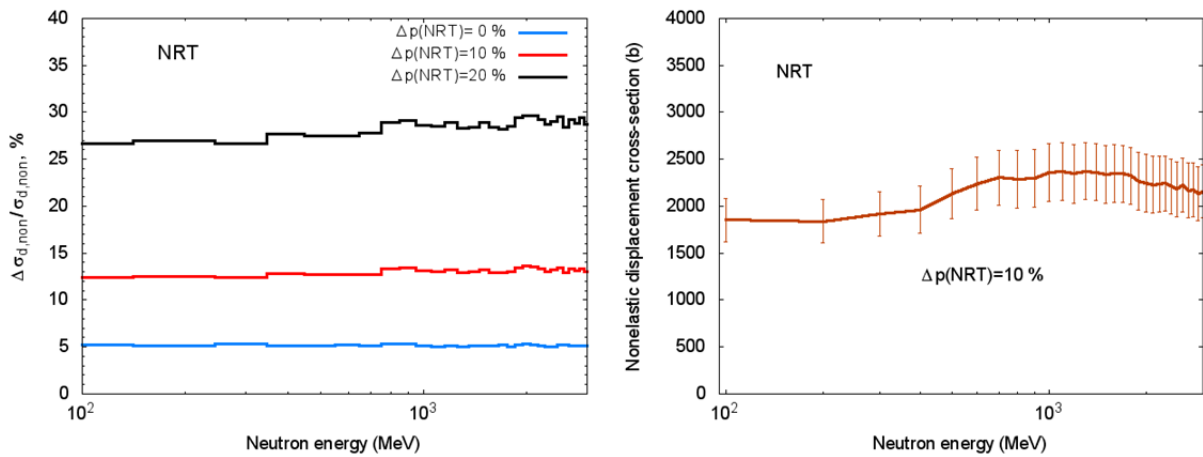


Fig.24 The RSD values of displacement cross-section for neutron nonelastic interactions with iron calculated using the CASCADE code applying the NRT model with different variation of NRT parameters (left) and the example of nonelastic displacement cross-section with error calculated with the RSD value of $\Delta p(\text{NRT})$ equal to 10%. The variation of nuclear model parameters is described in the text.

4. Conclusion

Uncertainty of displacement cross-section σ_d was evaluated for iron and tungsten irradiated with neutrons with energies from 0.1 MeV to 3 GeV. The TALYS [3] and ECIS [12] codes were applied for recoil energy distribution calculations in the energy range 0.1 to 150 MeV; the CASCADE code [4,5] implementing the intranuclear cascade evaporation model was used at the higher energies. Some results obtained in Ref.[17] using the MCNP code [15] and the DISCA-C code [14] were applied to get the uncertainty of calculated displacement cross-sections at neutron energies up to 3 GeV.

The NRT model [6,10] and the arc-dpa approach [8] were utilized to calculate the number of stable defects

The RSD-values and correlation matrices for σ_d were obtained for different variations of optical model parameters, nuclear level density parameters, and parameters of models describing the number of defects produced under irradiation. The results are shown in Figs.14, 21, and 24.

An additional study is needed to define the appropriate RSD values for the variation of NRT and arc-dpa parameters.

References

- [1] A.Yu. Konobeyev, U. Fischer, P.E. Pereslavl'tsev, S.P. Simakov, Uncertainties in the displacement cross-sections of Fe and W, EFFDOC-1180; https://www.oecd-nea.org/dbdata/nds_effdoc/effdoc-1180.pdf
- [2] D.L. Smith, Covariance matrices for nuclear cross sections derived from nuclear model calculations, ANL/NDM-159, Argonne National Laboratory, 2004
- [3] A.J. Koning, S. Hilaire, and M.C. Duijvestijn, TALYS, Proc. Int. Conf. on Nuclear Data for Science and Technology, April 22-27, 2007, Nice, France, 2008, p. 211; TALYS-1.8, <http://www.talys.eu/>
- [4] V.S. Barashenkov, Monte Carlo simulation of ionization and nuclear processes initiated by hadron and ion beams in media, *Comp. Phys. Comm.* **126** (2000) 28
- [5] A.Yu. Konobeyev, U. Fischer, Simulation of heavy cluster emission in nucleon induced reactions on targets from C to Bi at intermediate energies, KIT Scientific Reports 7684 (2014); <http://digbib.ubka.uni-karlsruhe.de/volltexte/1000043611>
- [6] M.J. Norgett, M.T. Robinson, I.M. Torrens, A proposed method of calculating displacement dose rates, *Nucl. Eng. Des.* **33** (1975) 50
- [7] K. Nordlund, A.E. Sand, F. Granberg, S.J. Zinkle, R. Stoller, R.S. Averback, T. Suzudo, L. Malerba, F. Banhart, W.J. Weber, F. Willaime, S. Dudarev, D. Simeone, Primary radiation damage in materials, NEA/NSC/DOC(2015)9, OECD 2015
- [8] K. Nordlund, Summary of the 2nd RCM of CRP on primary radiation damage cross-section. Summary report of the Second Research Coordination Meeting, 29 June - 2 July 2015, IAEA Headquarters, Vienna, Austria, INDC(NDS)- 0691, December 2015 p.19; <https://www-nds.iaea.org/publications/indc/indc-nds-0691.pdf>
- [9] M.T. Robinson, The energy dependence of neutron radiation damage in solids, Proc. Conf. on Nuclear Fusion Reactors, UKAEA Culham Lab. 17-19 Sept. 1969, eds. J.L. Hall and J.H.C. Maples (British Nuclear Energy Society, London, 1970) p. 364

- [10] M.T. Robinson, Basic physics of radiation damage production, *J. Nucl. Mater.* 216 (1994) 1
- [11] A.J. Koning, J.P. Delaroche, Local and global nucleon optical models from 1 keV to 200 MeV, *Nucl. Phys.* A713 (2003) 231
- [12] J. Raynal, ECIS96, Proc. Specialists' Meeting on the Nucleon Nucleus Optical Model up to 200 MeV, Bruyères-le-Chatel, France, Nov. 13-15, 1996, <http://www.nea.fr/html/science/om200/raynal.pdf>
- [13] A.J. Koning, D. Rochman, J. Kopecky, J.Ch. Sublet, M. Fleming, E. Bauge, S. Hilaire, P. Romain, B. Morillon, H. Duarte, S.C van der Marck, S. Pomp, H. Sjostrand, R. Forrest, H. Henriksson, O. Cabellos, S. Goriely, J. Leppanen, H. Leeb, A. Plompen, R. Mills, TENDL-2015; https://tendl.web.psi.ch/tendl_2015/tendl2015.html
- [14] C.H.M. Broeders, A. Yu. Konobeyev, Yu. A. Korovin, V. N. Sosnin, DISCA – advanced intranuclear cascade cluster evaporation model code system for calculation of particle distributions and cross sections, FZKA 7221 (2006); <http://d-nb.info/98154746X/34>
- [15] J.T. Goorley, M.R. James, T.E. Booth, F.B. Brown, J.S. Bull, L.J. Cox, J.W. Durkee, J.S. Elson, M.L. Fensin, R. A. Forster, J.S. Hendricks, H.G. Hughes, R.C. Johns, B.C. Kiedrowski, R.L. Martz, S.G. Mashnik, G.W. McKinney, D.B. Pelowitz, R.E. Prael, J.E. Sweezy, L.S. Waters, T.A. Wilcox, A. Zukaitis, MCNP6TM User's manual, Ed. D.B. Pelowitz, LA-CP-13-00634, May 2013
- [16] A.Yu. Konobeyev, C.H.M. Broeders, U. Fischer, Improved displacement cross sections for structural materials irradiated with intermediate and high energy protons, Proc. 8th International Topical Meeting on the Nuclear Applications of Accelerator Technology (AccApp'07), July 30 - August 2, 2007, Pocatello, Idaho, USA, p.241
- [17] A.Yu. Konobeyev, U. Fischer, L. Zanini, Advanced evaluations of displacement and gas production cross sections for chromium, iron, and nickel up to 3 GeV incident particle energy, Tenth International Topical Meeting on Nuclear Applications of Accelerators (AccApp'11), Knoxville, TN April 3-7, 2011

Appendix A

Results of ECIS code calculations for iron using the Koning-Delarocche optical potential: shape elastic scattering cross-section, total cross-section, shape elastic component of displacement cross-section, and corresponding RSD-values obtained using the NRT model and the arc-dpa approach. The results shown in Figs.A1-A11 are obtained with the variation of V , W , and W_d -parameters of the optical potential and the results in Figs.A12,A13 with additional variation of other parameters. See details in Section 2.1.1.1.

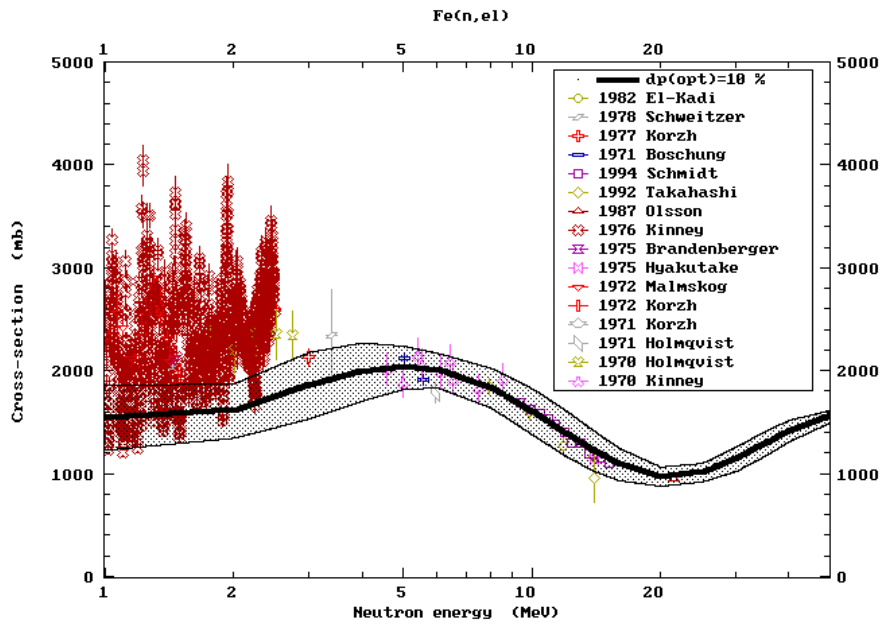


Fig.A1* Shape elastic scattering cross-section for iron, $\Delta p(\text{opt})$ is equal to 10 %.

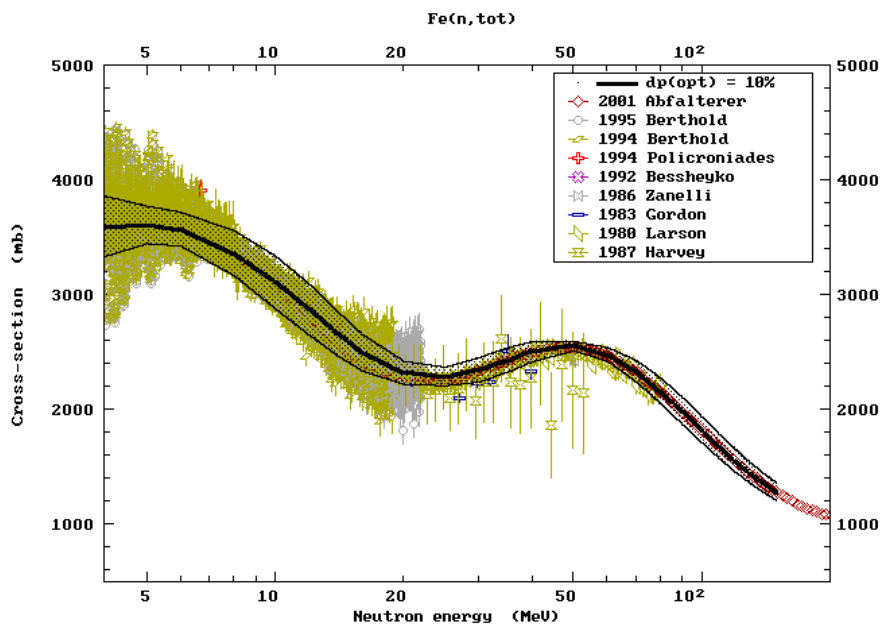


Fig.A2* Total cross-section for iron, $\Delta p(\text{opt})$ is equal to 10 %.

*The graph was prepared using the ZVView-system, <https://www-nds.iaea.org/public/zvview/>

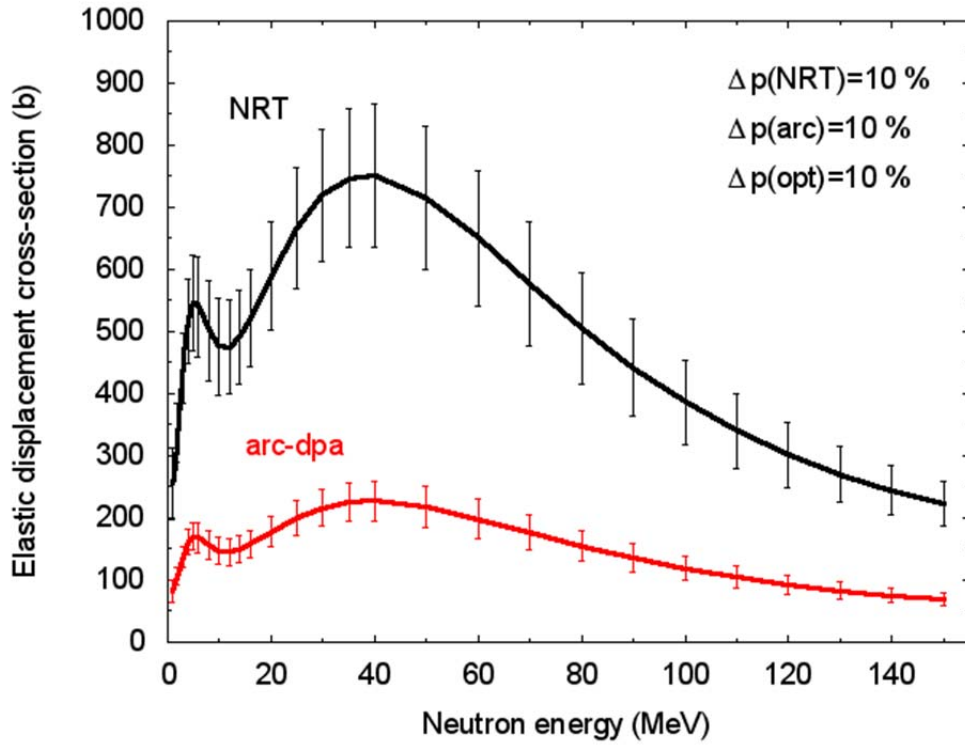


Fig.A3 Shape elastic component of displacement cross-section for iron.

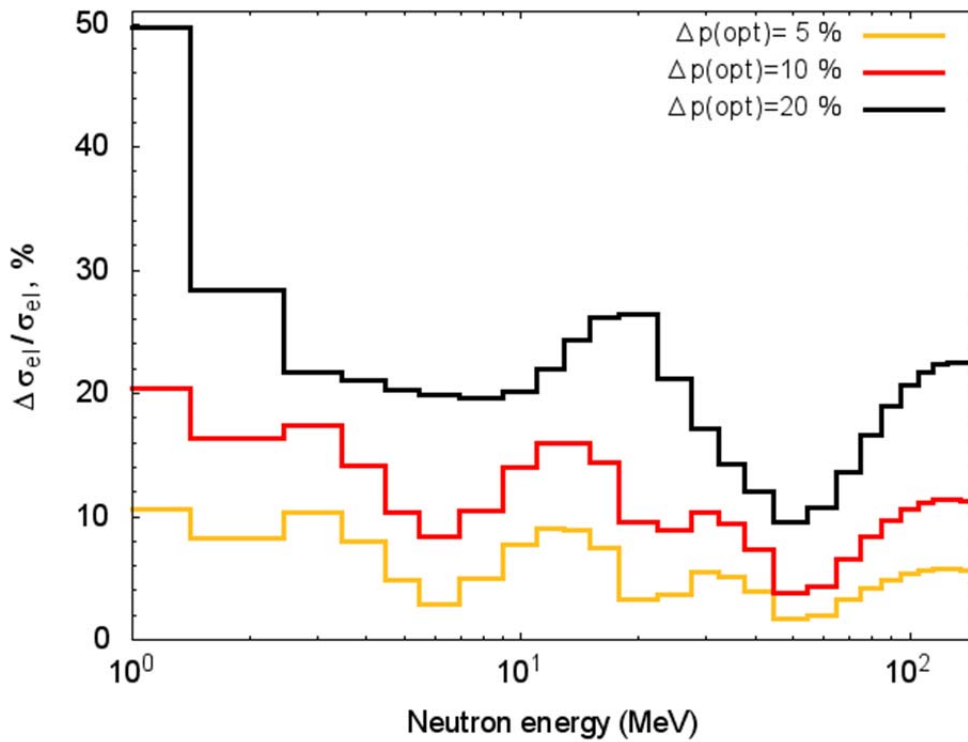


Fig.A4 The RSD values of shape elastic scattering cross-section calculated with different variation of optical model parameters for iron.

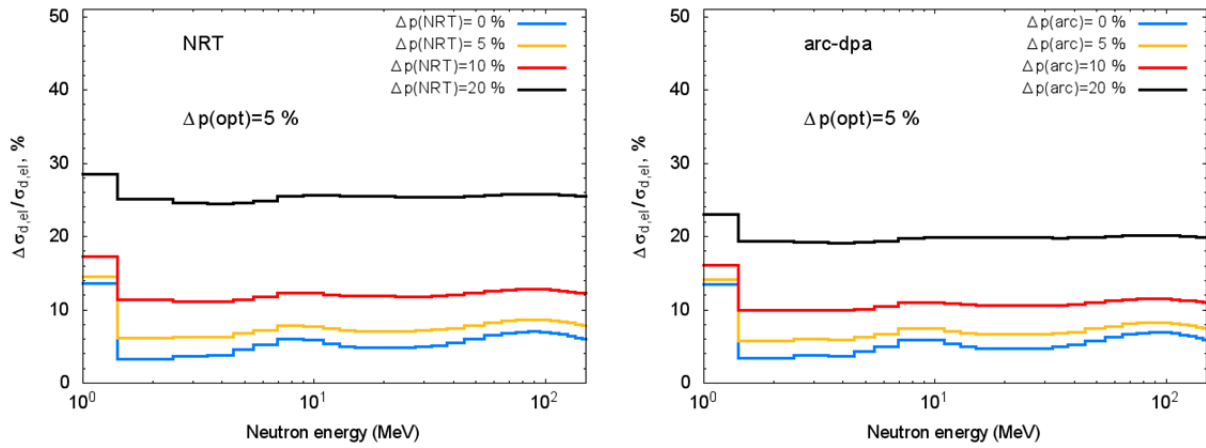


Fig.A5 The RSD values of displacement cross-section concerning the shape elastic scattering for iron calculated using the NRT model (left) and the arc-dpa approach (right) with different variation of NRT and arc-dpa parameters and the variation of optical model parameters with RSD value $\Delta p(\text{opt})$ equal to 5%.

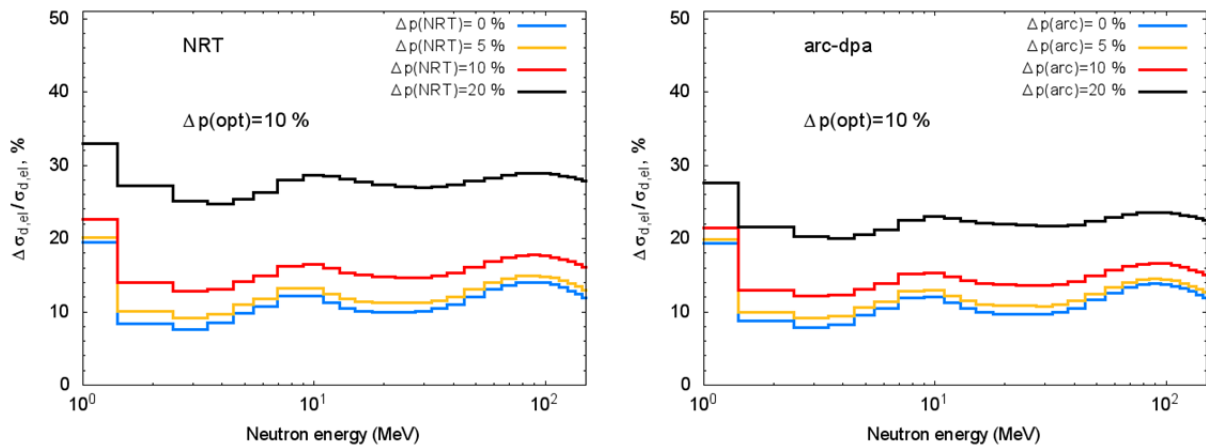


Fig.A6 The same as in Fig.A5 with $\Delta p(\text{opt})$ equal to 10%.

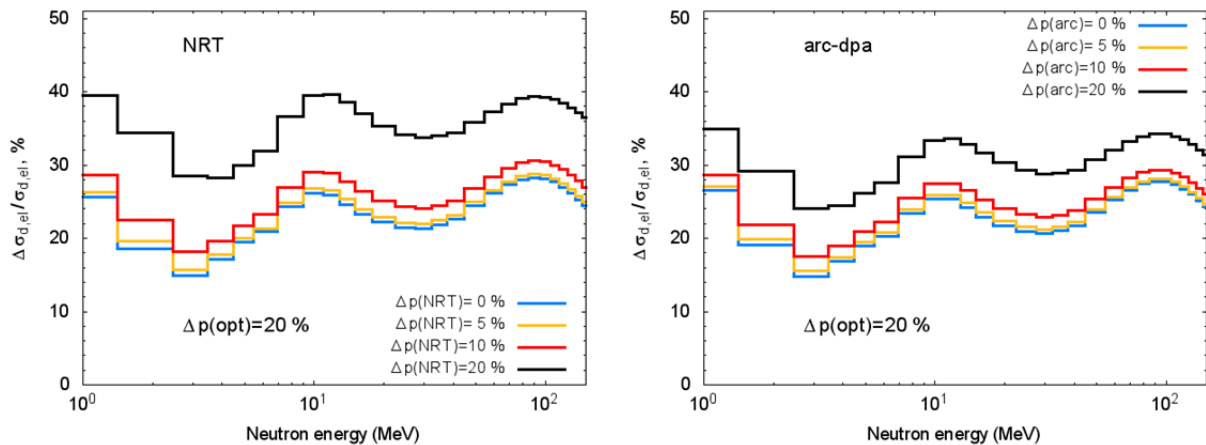


Fig.A7 The same as in Fig.A5 with $\Delta p(\text{opt})$ equal to 20%.

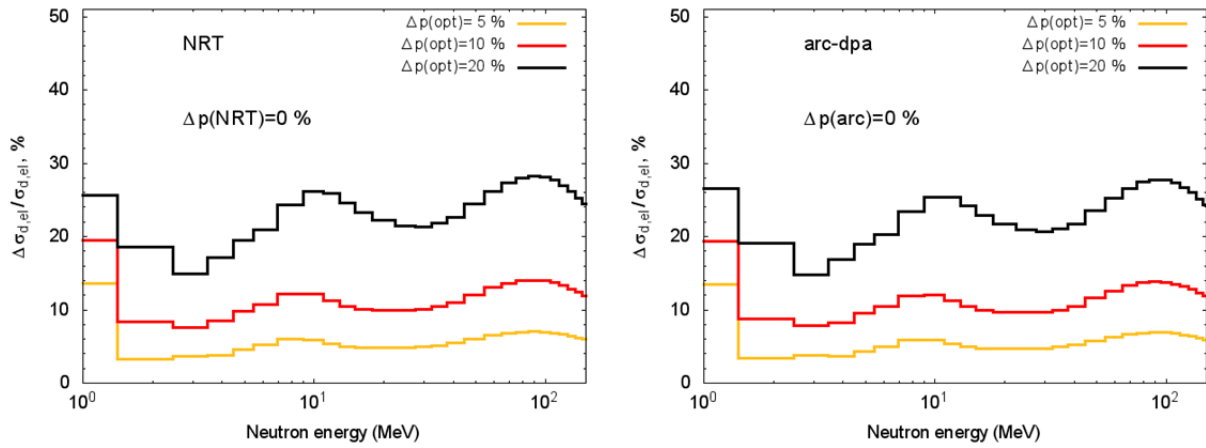


Fig.A8 The RSD values of displacement cross-section concerning the shape elastic scattering for iron calculated using the NRT model (left) and the arc-dpa approach (right) with different variation of optical model parameters and without the variation of NRT and arc-dpa parameters.

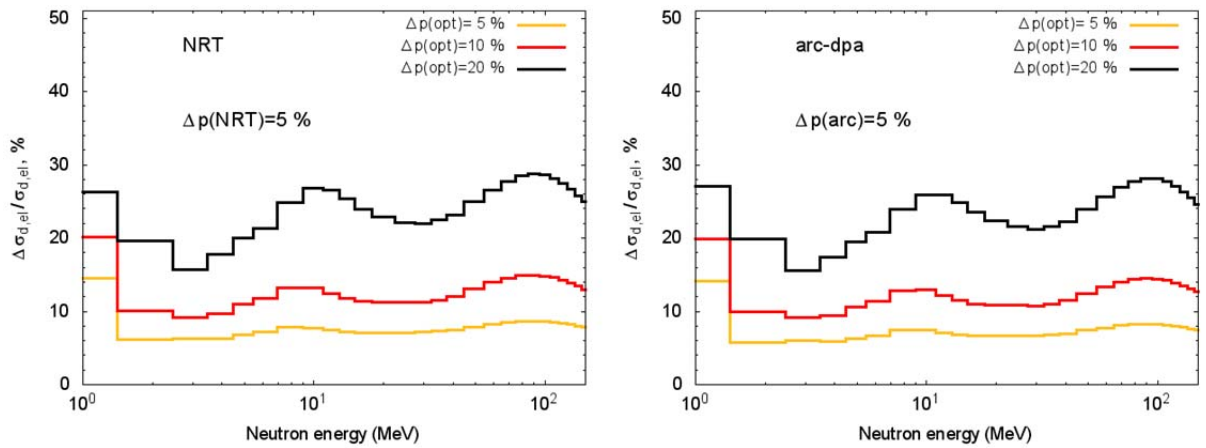


Fig.A9 The RSD values of displacement cross-section concerning the shape elastic scattering for iron calculated using the NRT model (left) and the arc-dpa approach (right) with different variation of optical model parameters and the variation of NRT and arc-dpa parameters with RSD value equal to 5%.

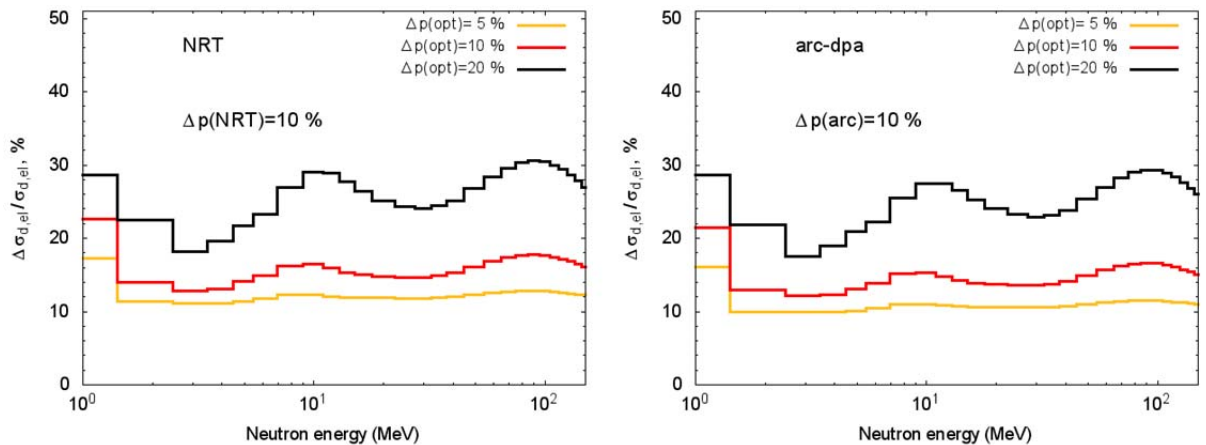


Fig.A10 The same as in Fig.A9 with $\Delta p(\text{NRT})$ and $\Delta p(\text{arc})$ equal to 10%.

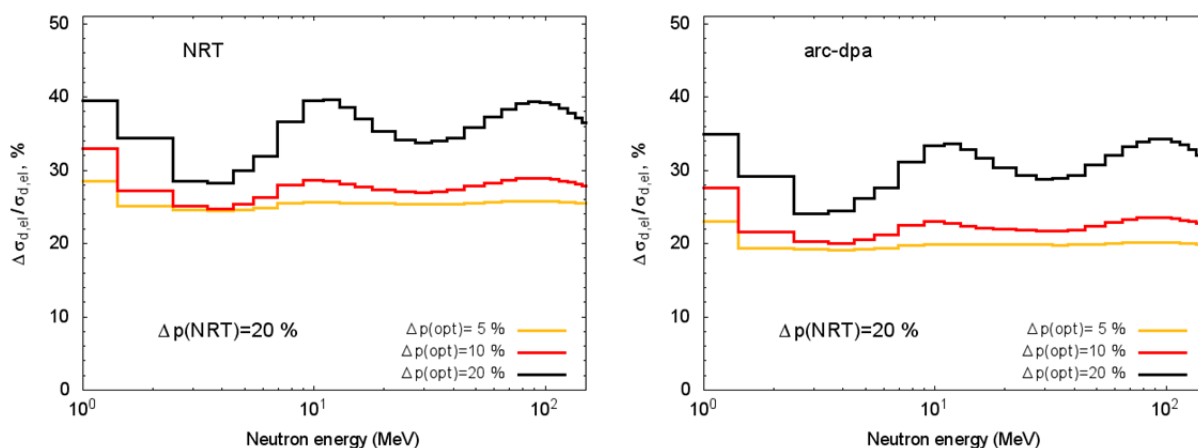


Fig.A11 The same as in Fig.A9 with $\Delta p(\text{NRT})$ and $\Delta p(\text{arc})$ equal to 20%.

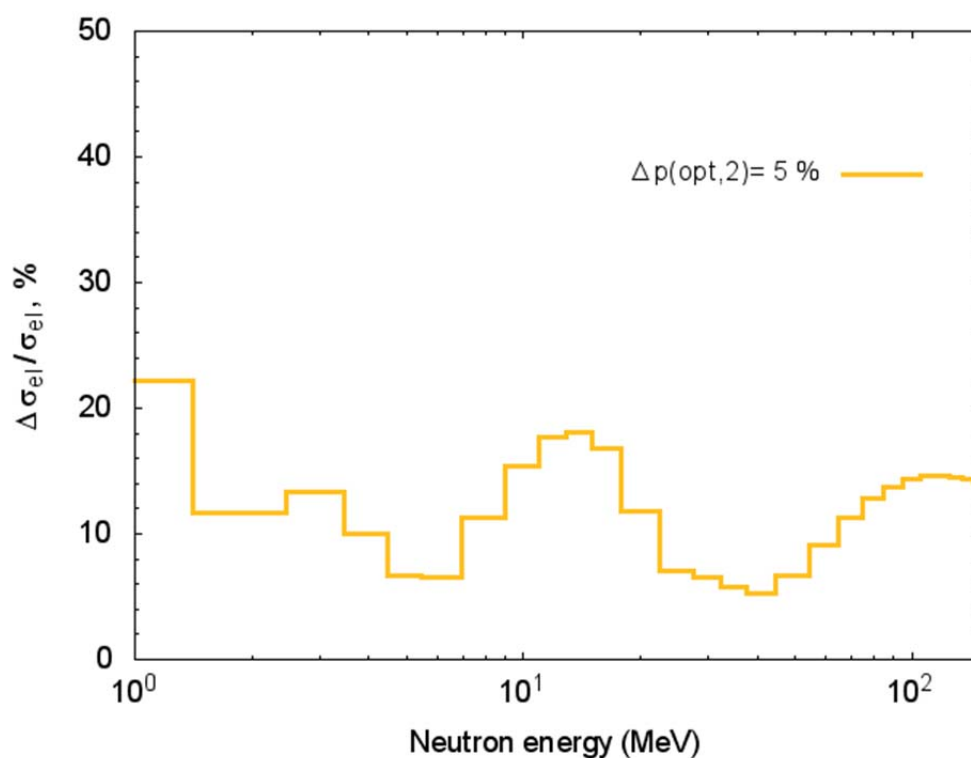


Fig.A12 The RSD values of shape elastic scattering cross-section for iron calculated with the variation of optical model parameters with RSD value equal to 5%. All input variable of the ECIS code were varied. See explanations in the text.

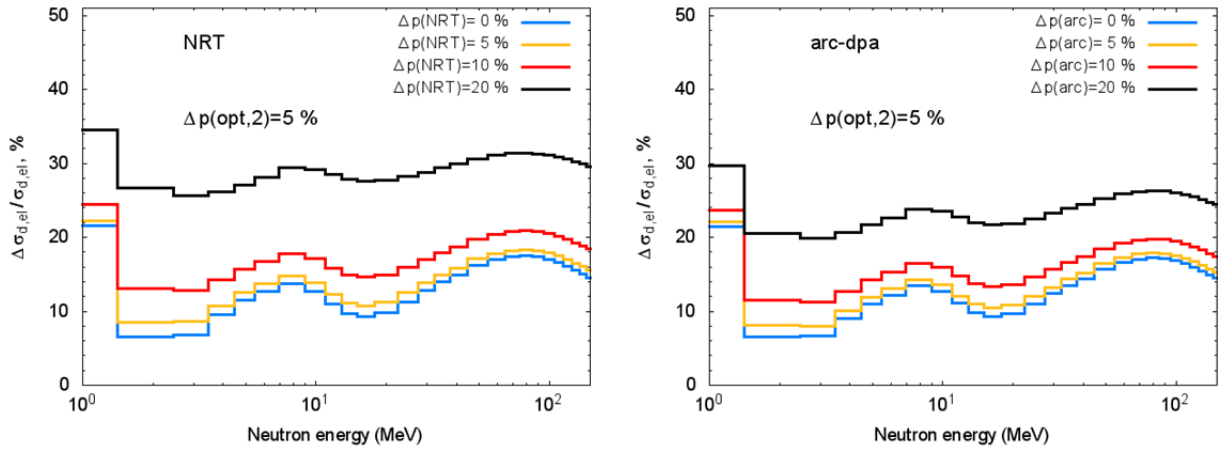


Fig.A13 The RSD values of displacement cross-section concerning the shape elastic scattering for iron calculated using the NRT model (left) and the arc-dpa approach (right) with different variation of NRT and arc-dpa parameters and the variation of optical model parameters with RSD value equal to 5%. All input variable of the ECIS code were varied. See explanations in the text.

Appendix B

The RSD values of elastic scattering (shape elastic and compound) component of displacement cross-section for iron calculated using the TALYS code at primary neutron energies from 0.1 up to 150 MeV

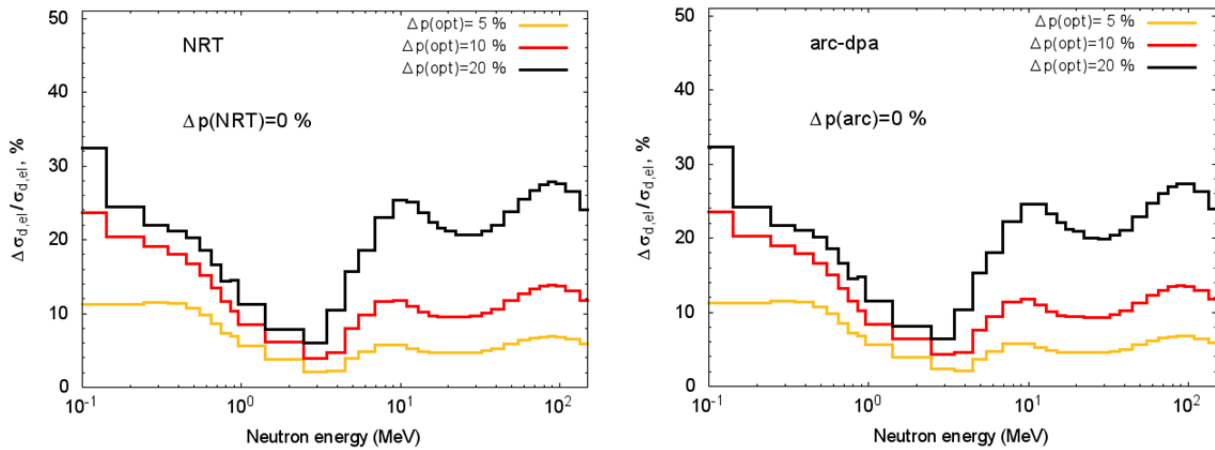


Fig.B1 The RSD values of elastic scattering (shape elastic and compound) component of displacement cross-section for iron calculated using the NRT model (left) and the arc-dpa approach (right) with different variation of optical model parameters and without the variation of NRT and arc-dpa parameters.

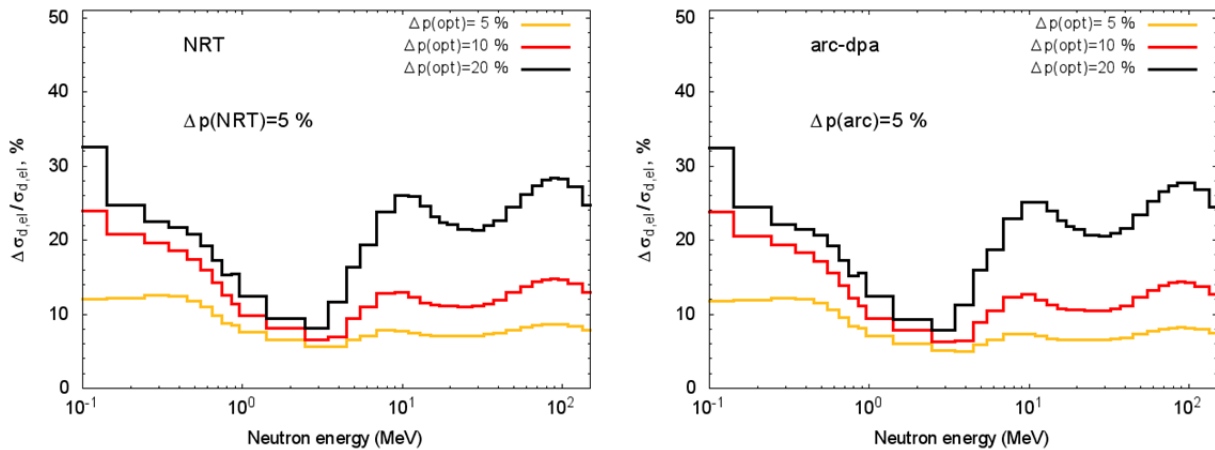


Fig.B2 The RSD values of elastic scattering component of displacement cross-section for iron calculated using the NRT model (left) and the arc-dpa approach (right) with different variation of optical model parameters and the variation of NRT and arc-dpa parameters with the RSD value equal to 5%.

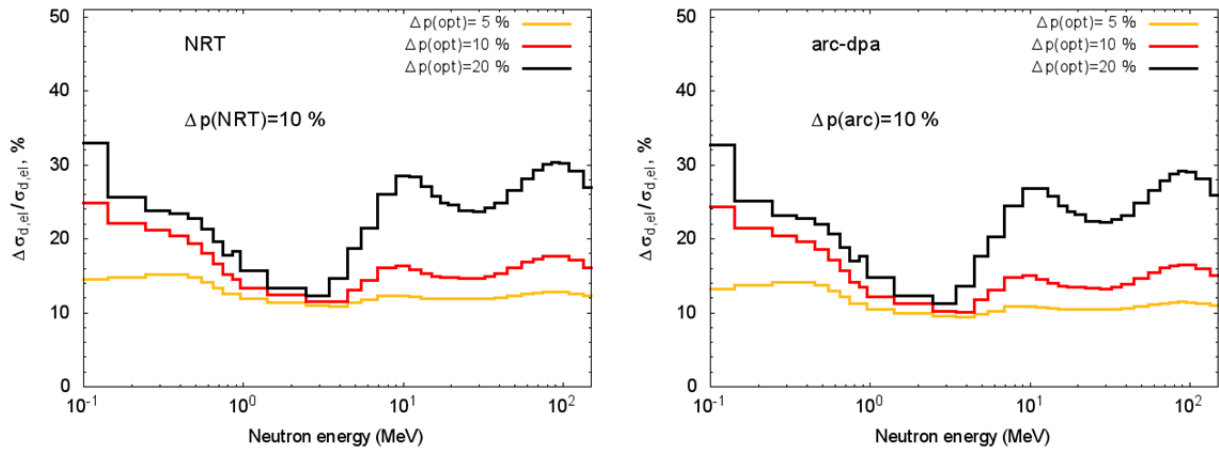


Fig.B3 The same as in Fig.B2 with $\Delta p(\text{NRT})$ and $\Delta p(\text{arc})$ values equal to 10%.

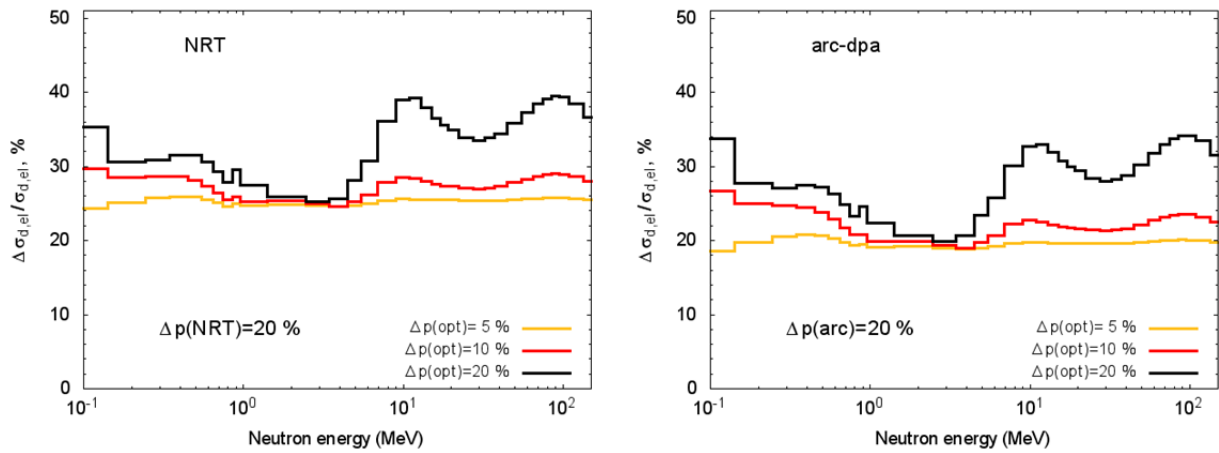


Fig.B4 The same as in Fig.B2 with $\Delta p(\text{NRT})$ and $\Delta p(\text{arc})$ values equal to 20%.

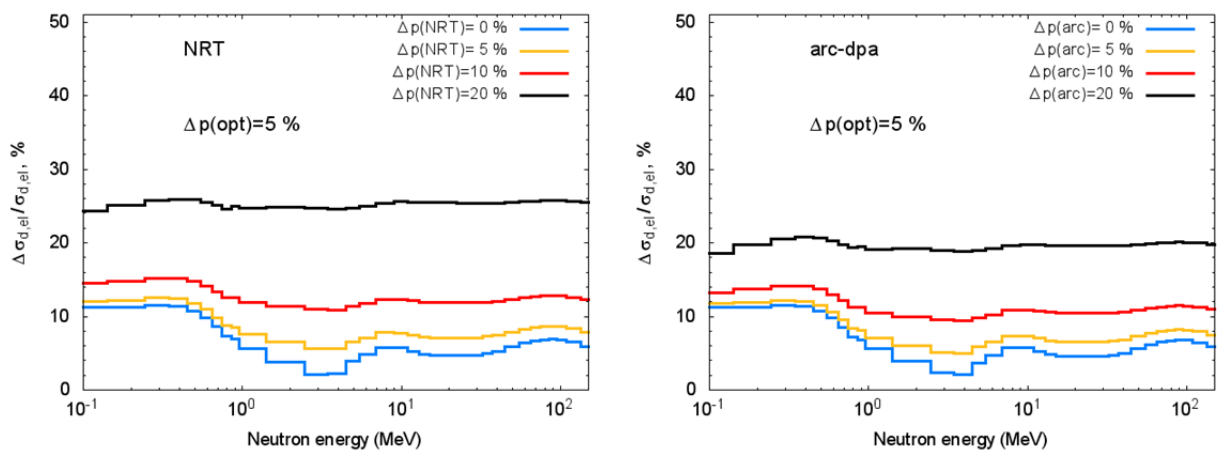


Fig.B5 The RSD values of elastic scattering component of displacement cross-section for iron calculated using the NRT model (left) and the arc-dpa approach (right) with different variation of NRT and arc-dpa parameters and variation of optical model parameters with the RSD value $\Delta p(\text{opt})$ equal to 5%.

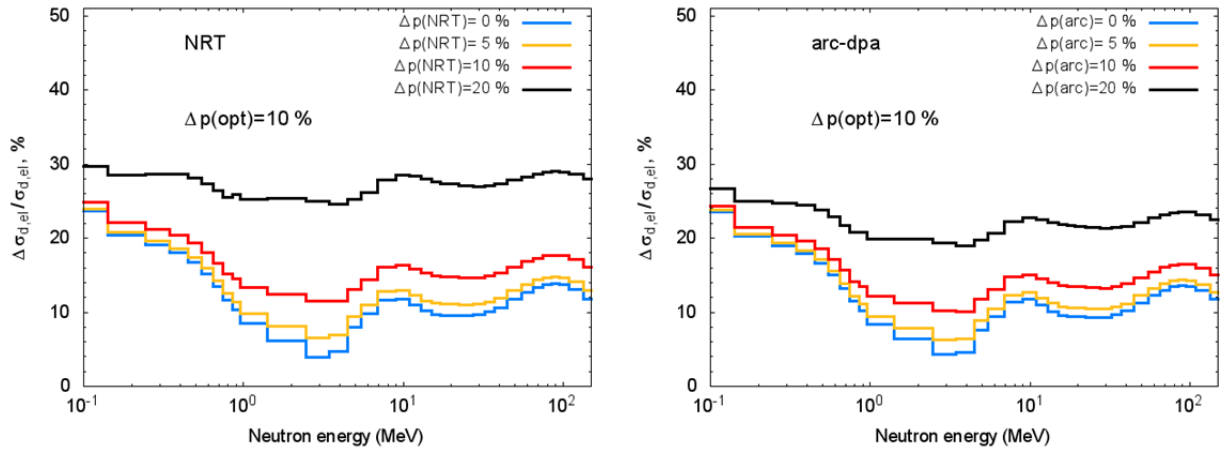


Fig.B6 The same as in Fig.B5 with $\Delta p(\text{opt})$ equal to 10%.

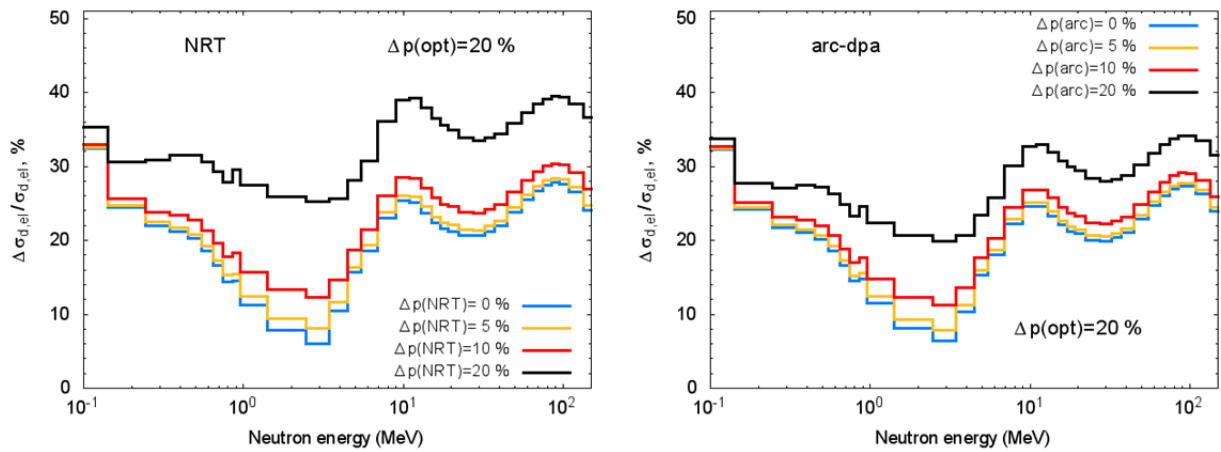


Fig.B7 The same as in Fig.B5 with $\Delta p(\text{opt})$ equal to 20%.

Appendix C

The RSD values of inelastic discrete-level scattering component of displacement cross-section for iron calculated using the TALYS code at primary neutron energies up to 150 MeV

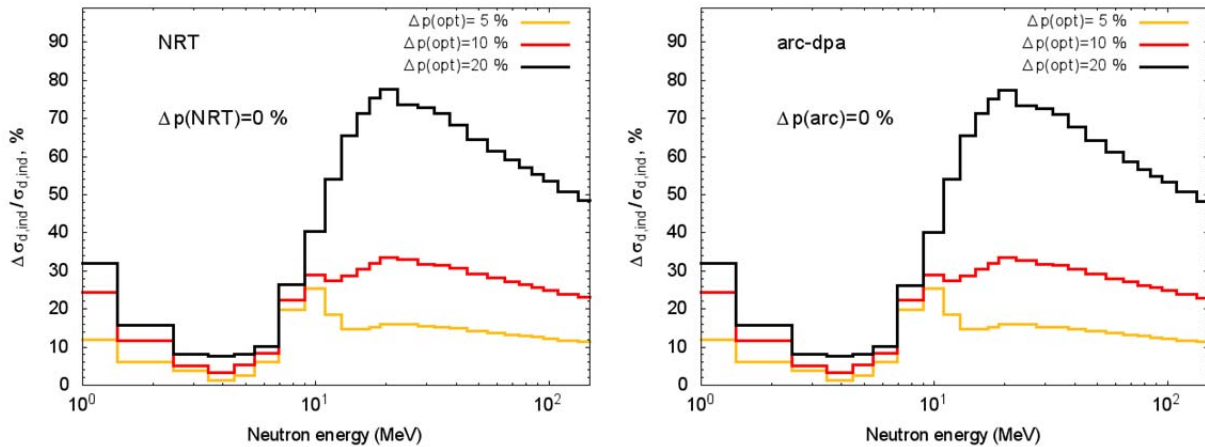


Fig.C1 The RSD values of inelastic discrete-level scattering component of displacement cross-section for iron calculated using the NRT model (left) and the arc-dpa approach (right) with different variation of optical model parameters and without the variation of NRT and arc-dpa parameters.

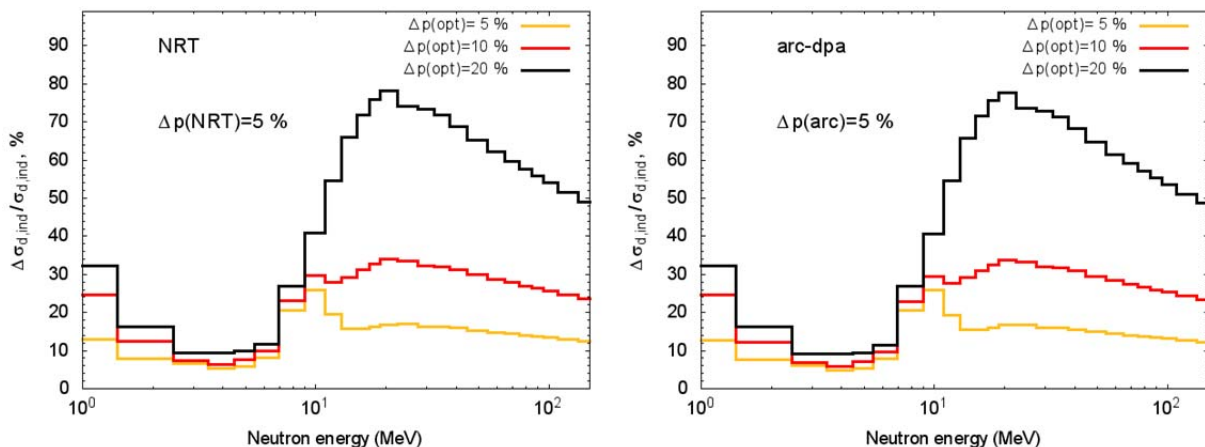


Fig.C2 The RSD values of inelastic discrete-level scattering component of displacement cross-section for iron calculated using the NRT model (left) and the arc-dpa approach (right) with different variation of optical model parameters and the variation of NRT and arc-dpa parameters with the RSD value equal to 5%.

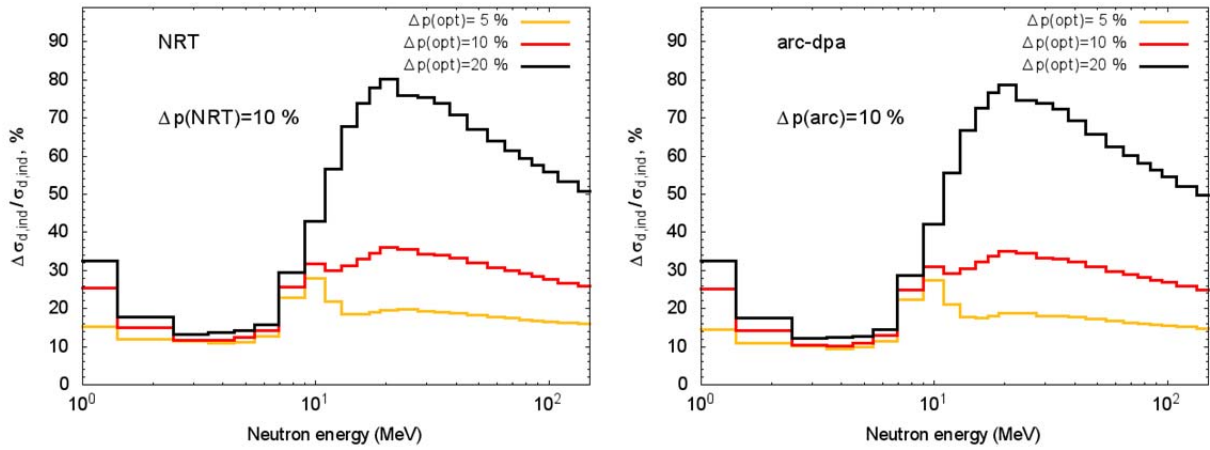


Fig.C3 The same as in Fig.C2 with $\Delta p(\text{NRT})$ and $\Delta p(\text{arc})$ values equal to 10%.

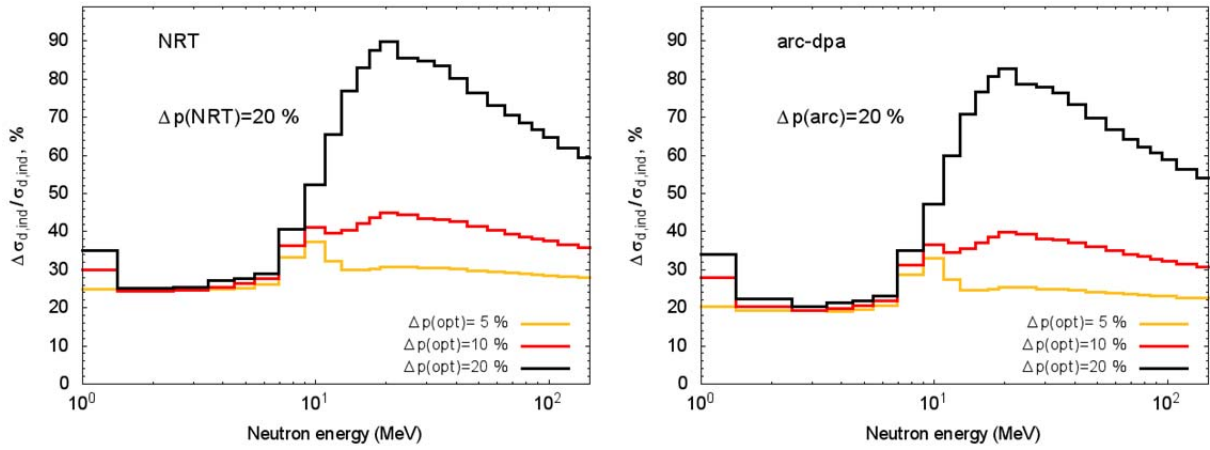


Fig.C4 The same as in Fig.C2 with $\Delta p(\text{NRT})$ and $\Delta p(\text{arc})$ values equal to 20%.

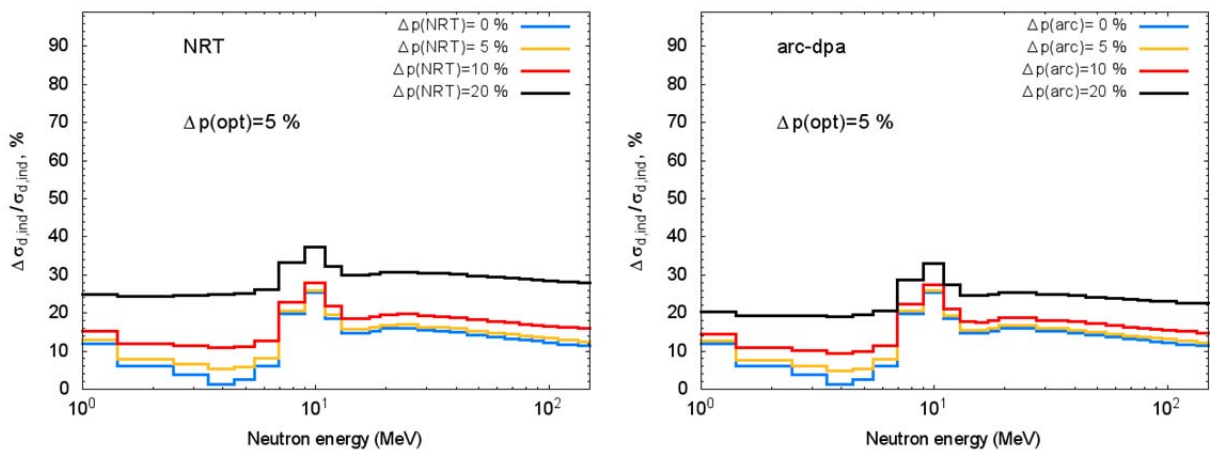


Fig.C5 The RSD values of inelastic discrete-level scattering component of displacement cross-section for iron calculated using the NRT model (left) and the arc-dpa approach (right) with different variation of NRT and arc-dpa parameters and variation of optical model parameters with the RSD value $\Delta p(\text{opt})$ equal to 5%.

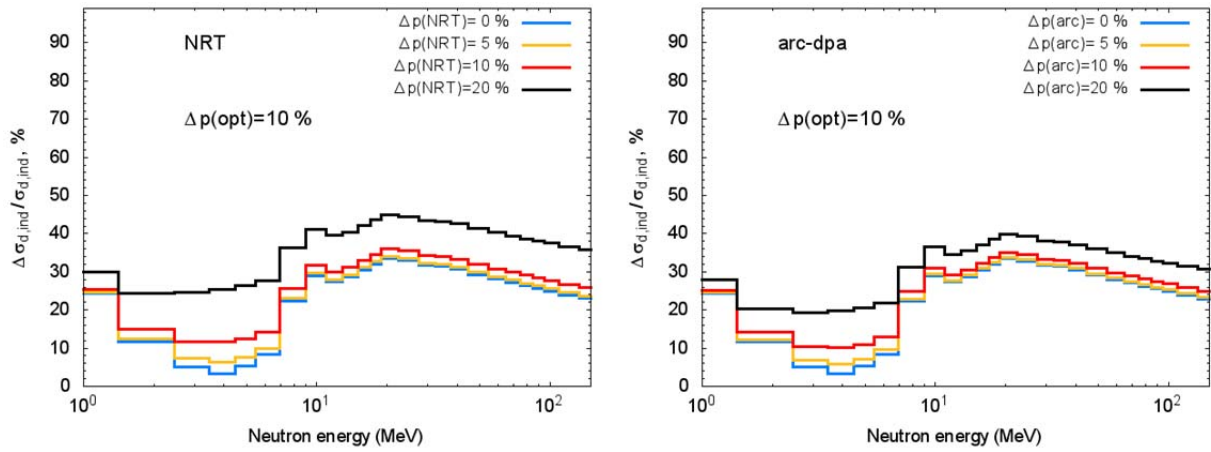


Fig.C6 The same as in Fig.C5 with $\Delta p(\text{opt})$ equal to 10%.

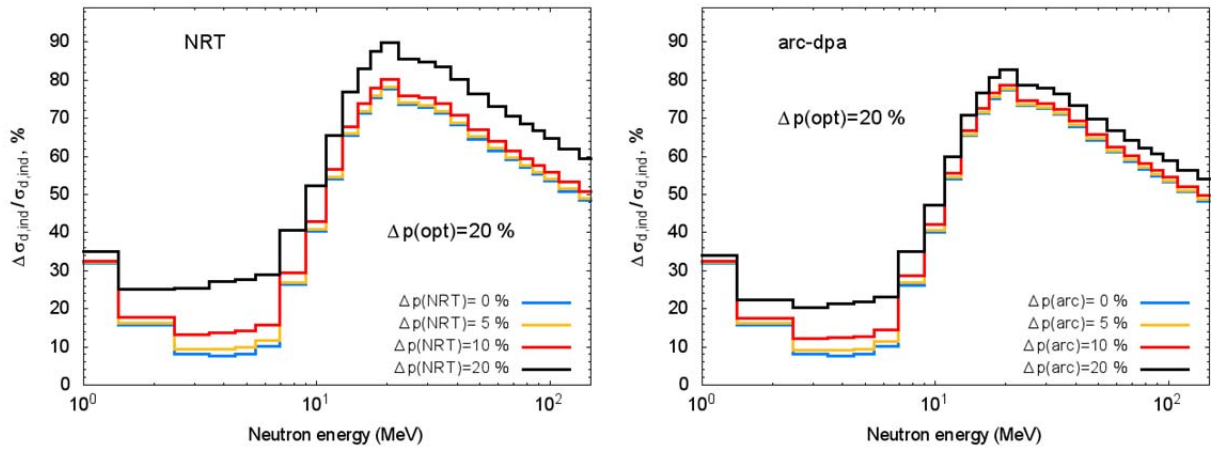


Fig.C7 The same as in Fig.C5 with $\Delta p(\text{opt})$ equal to 20%.

Appendix D

Examples of RSD values of cross-sections and displacement cross-sections for (n,np) and (n,3n) reactions for iron calculated using the TALYS code at primary neutron energies up to 150 MeV

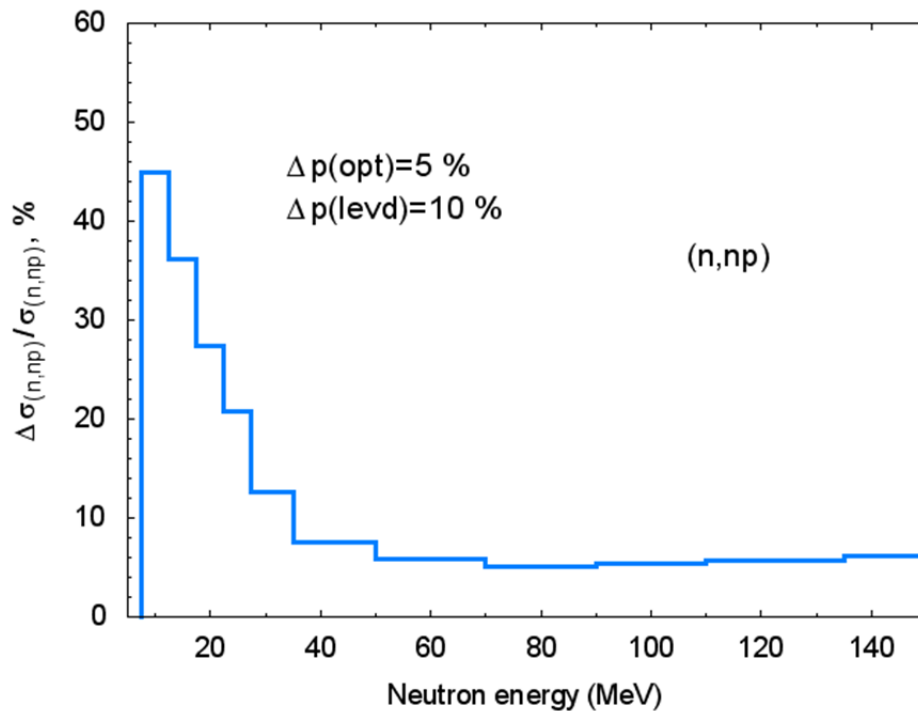


Fig.D1 The RSD values of (n,np) reaction cross-section calculated for iron.

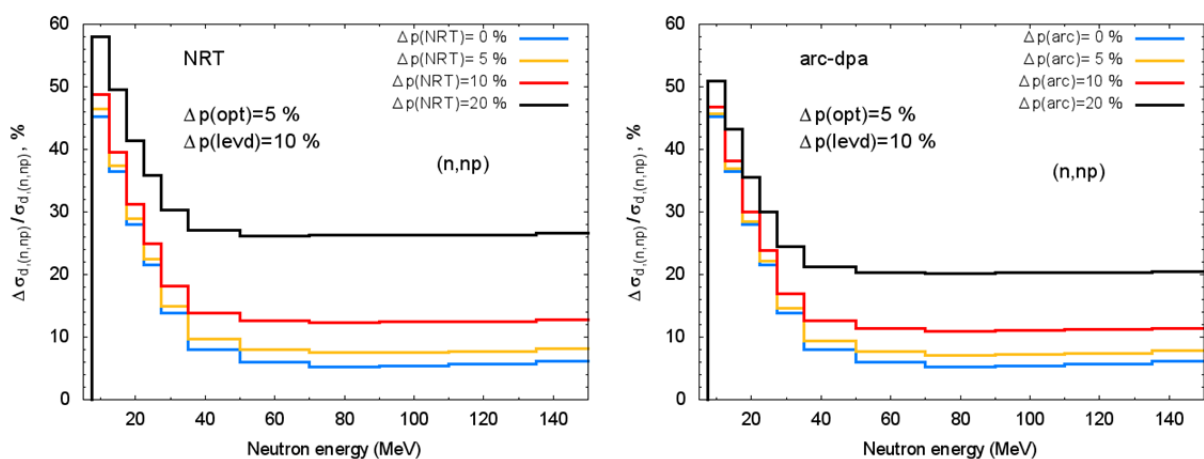


Fig.D2 The RSD values of (n,np) reaction component of displacement cross-section for iron calculated using the NRT model (left) and the arc-dpa approach (right) with different variation of NRT and arc-dpa parameters.

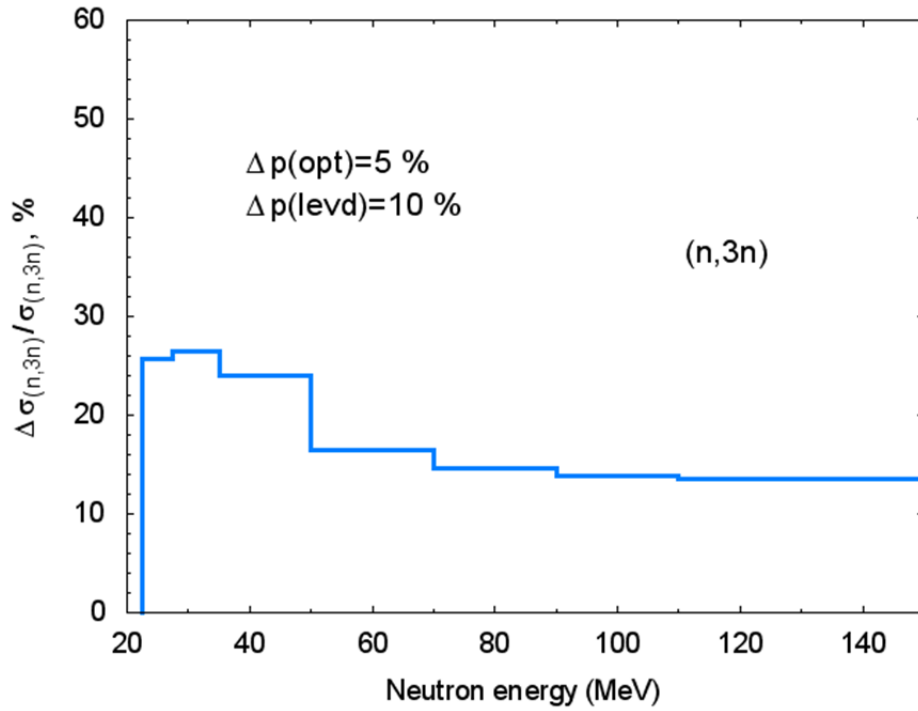


Fig.D3 The RSD values of (n,3n) reaction cross-section calculated for iron.

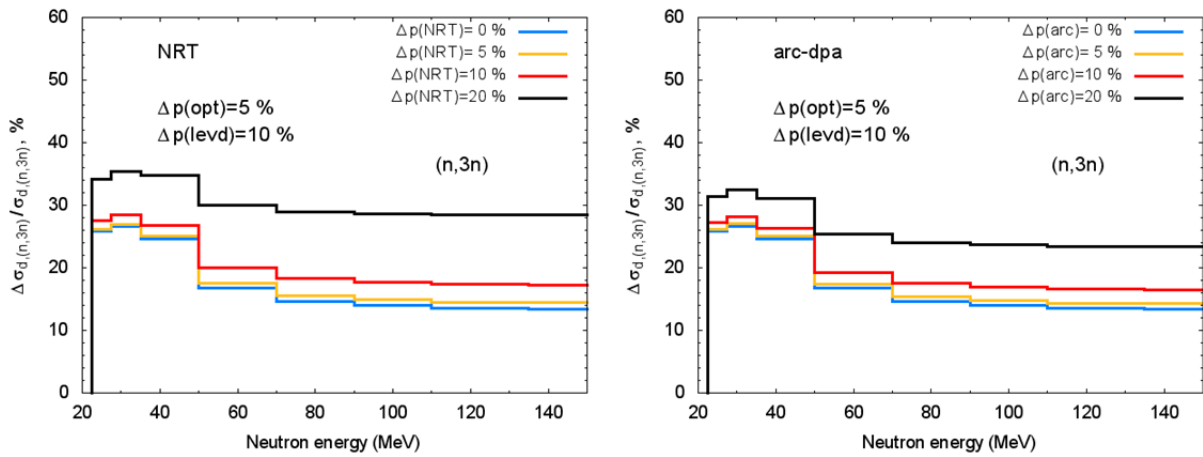


Fig.D4 The RSD values of (n,3n) reaction component of displacement cross-section for iron calculated using the NRT model (left) and the arc-dpa approach (right) with different variation of NRT and arc-dpa parameters.

Appendix E

The RSD values of elastic scattering (shape elastic and compound), inelastic discrete-level scattering, (n,2n), (n,np), and (n,3n) reaction cross-section and corresponding components of displacement cross-section for tungsten calculated using the TALYS code at primary neutron energies up to 150 MeV

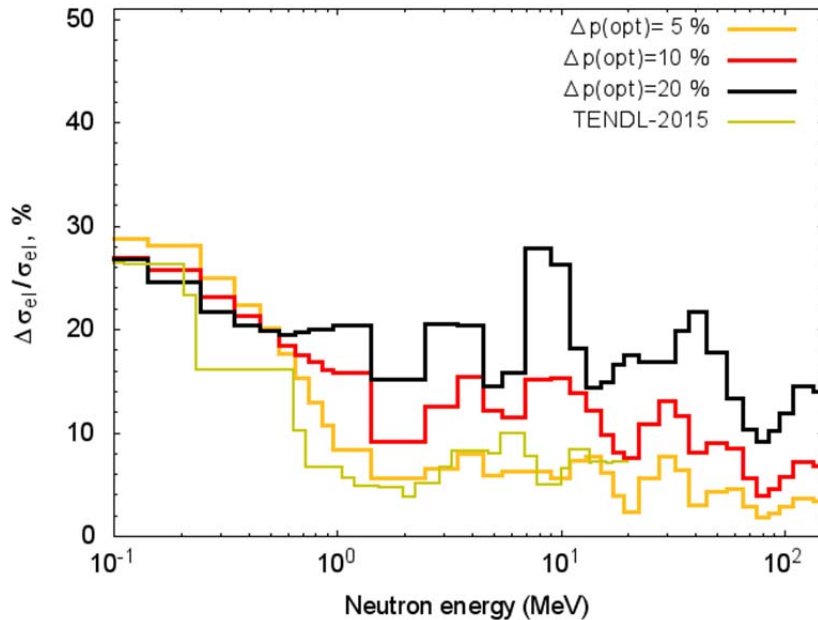


Fig.E1 The RSD values of elastic scattering (shape elastic and compound) cross-section for tungsten calculated with different variation of optical model parameters and TENDL-2015 data.

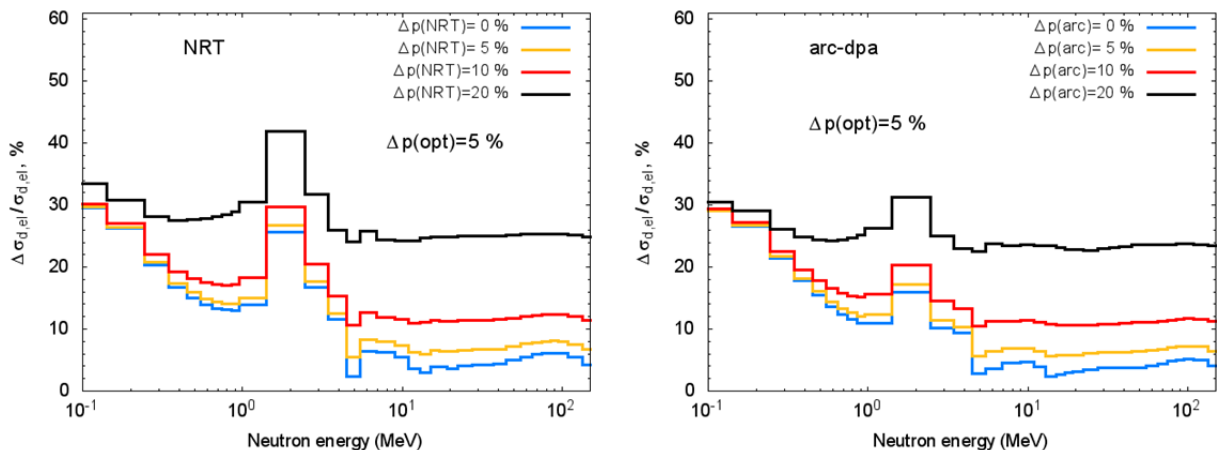


Fig.E2 The RSD values of elastic scattering (shape elastic and compound) component of displacement cross-section for tungsten calculated using the NRT model (left) and the arc-dpa approach (right) with different variation of NRT and arc-dpa parameters and the variation of optical model parameters with the RSD value $\Delta p(\text{opt})$ equal to 5%.

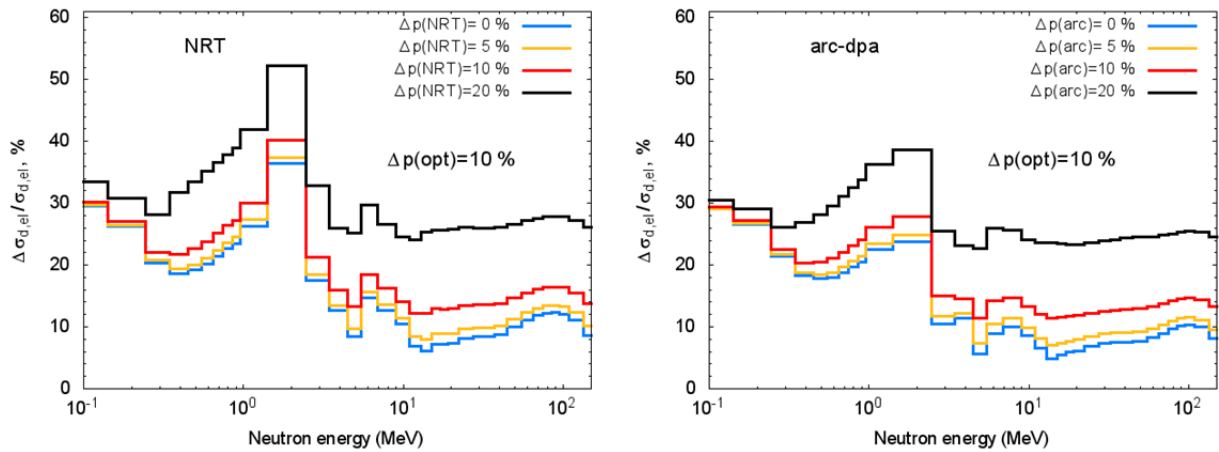


Fig.E3 The same as in Fig.E2 for $\Delta p(\text{opt})$ equal to 10%.

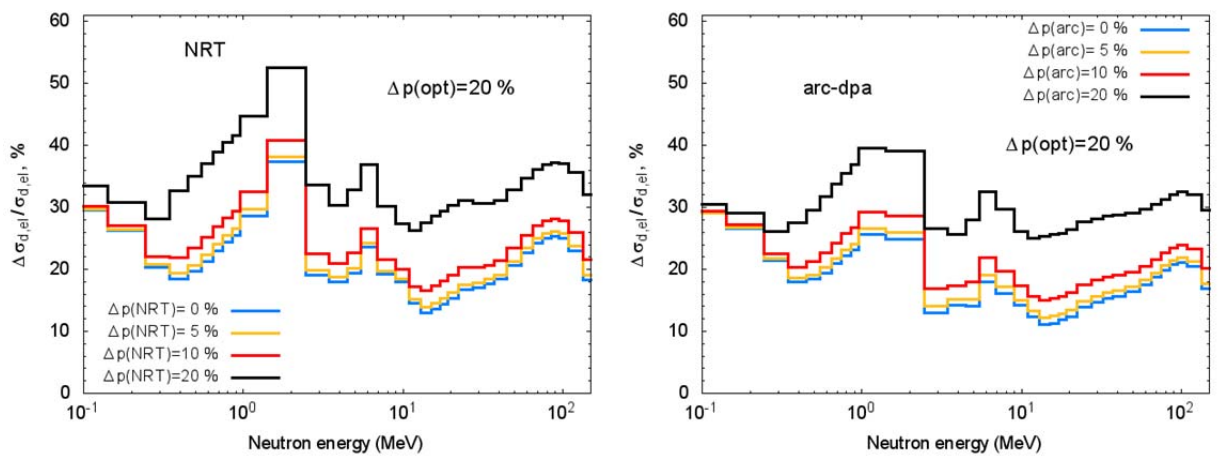


Fig.E4 The same as in Fig.E2 for $\Delta p(\text{opt})$ equal to 20%.

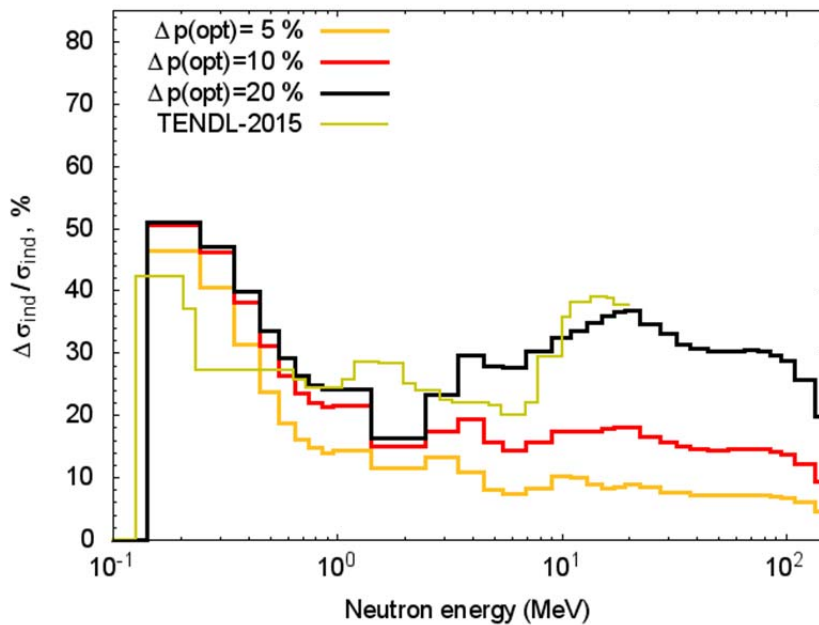


Fig.E5 The RSD values of inelastic discrete-level scattering cross-section for tungsten and TENDL-2015 data*.

* Data from TENDL-2015 correspond to MT=4 section of the ENDF/B file

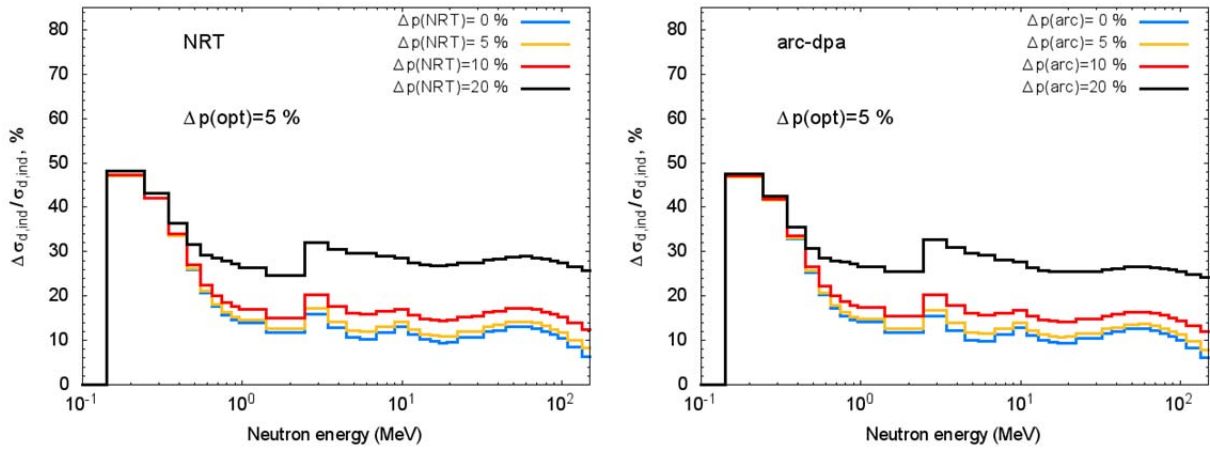


Fig.E6 The RSD values of inelastic discrete-level scattering component of displacement cross-section for tungsten calculated using the NRT model (left) and the arc-dpa approach (right) with different variation of NRT and arc-dpa parameters and the variation of optical model parameters with the RSD value $\Delta p(\text{opt})$ equal to 5%.

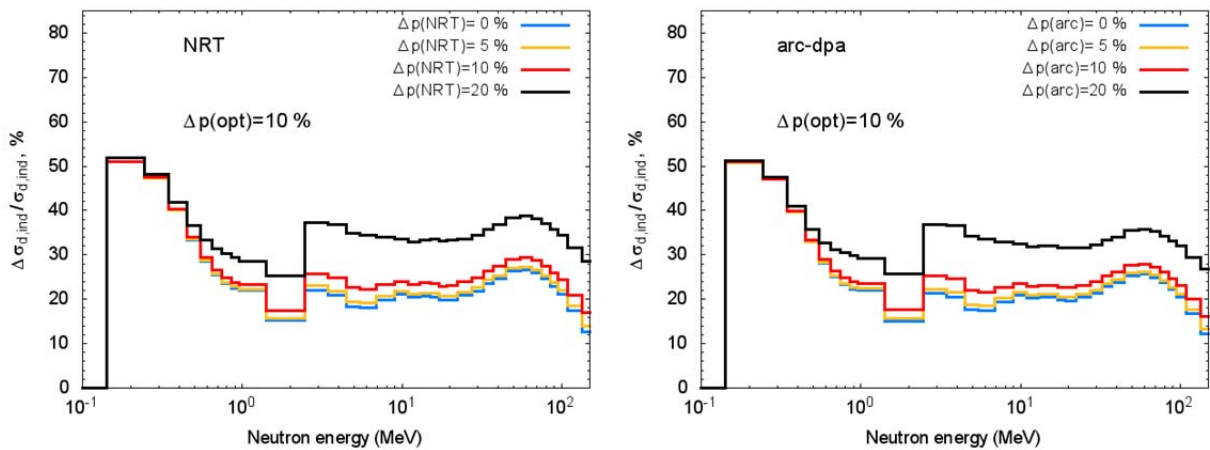


Fig.E7 The same as in Fig.E6 for $\Delta p(\text{opt})$ equal to 10%.

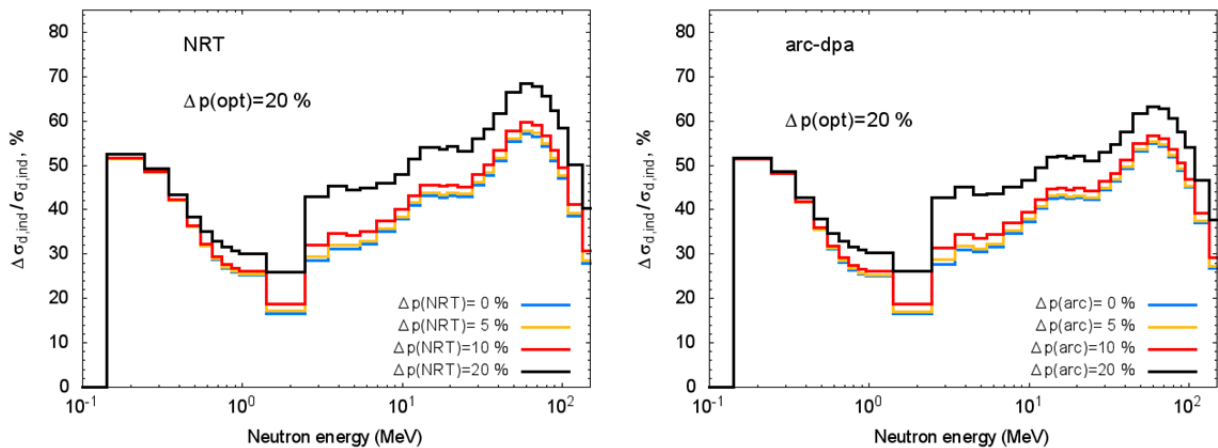


Fig.E8 The same as in Fig.E6 for $\Delta p(\text{opt})$ equal to 20%.

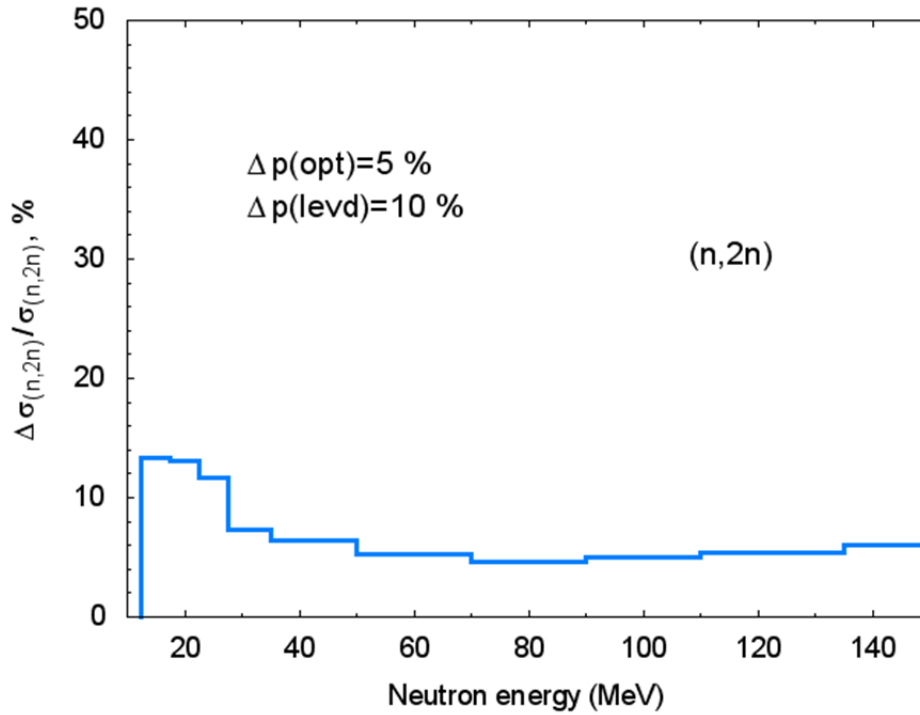


Fig.E9 The calculated RSD values of (n,2n) reaction cross-section for tungsten obtained with the variation of optical model and nuclear level density parameters with the RSD values equal to 5% and 10%, correspondingly.

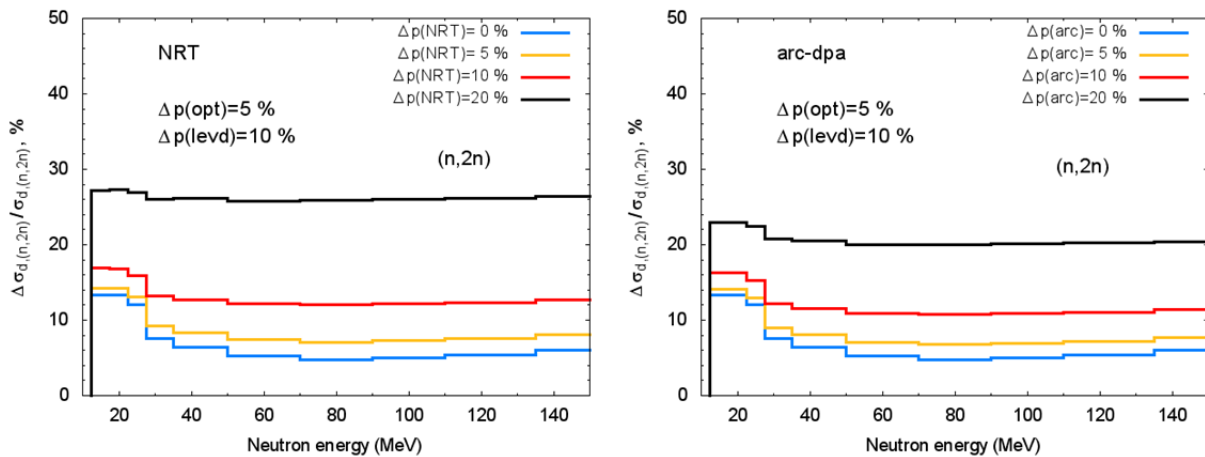


Fig.E10 The RSD values of (n,2n) reaction component of displacement cross-section for tungsten calculated using the NRT model (left) and the arc-dpa approach (right) with different variation of NRT and arc-dpa parameters, and the variation of optical model and nuclear level density parameters with the RSD values equal to 5% and 10%, correspondingly.

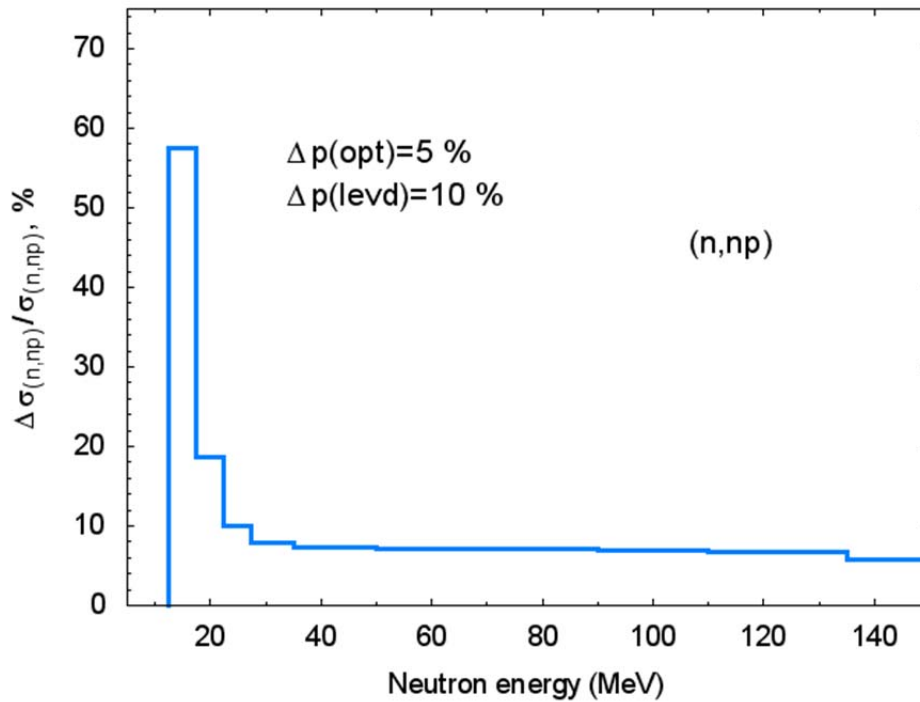


Fig.E11 The calculated RSD values of (n,np) reaction cross-section for tungsten obtained with the variation of optical model and nuclear level density parameters with the RSD values equal to 5% and 10%, correspondingly.

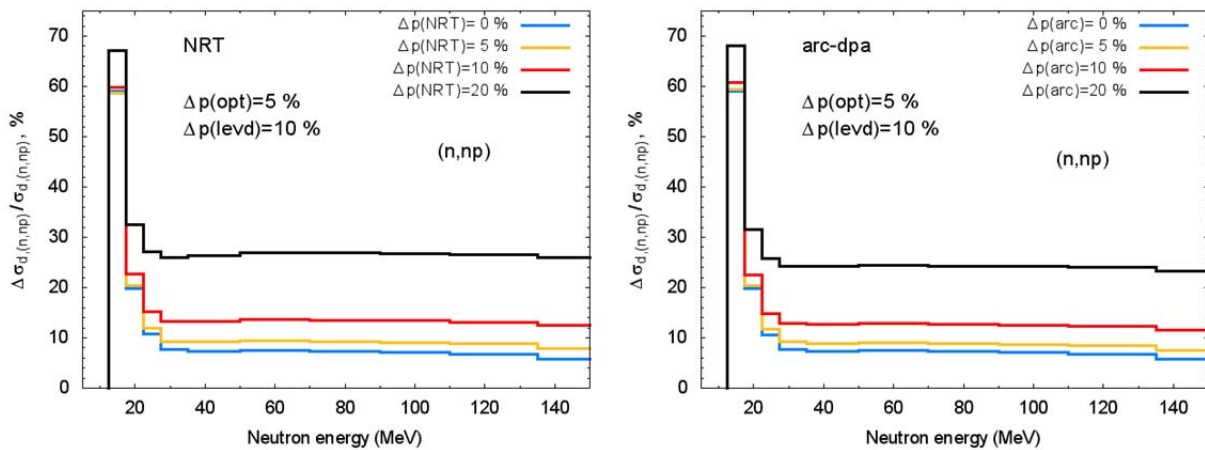


Fig.E12 The RSD values of (n,np) reaction component of displacement cross-section for tungsten calculated using the NRT model (left) and the arc-dpa approach (right) with different variation of NRT and arc-dpa parameters, and the variation of optical model and nuclear level density parameters with the RSD values equal to 5% and 10%, correspondingly.

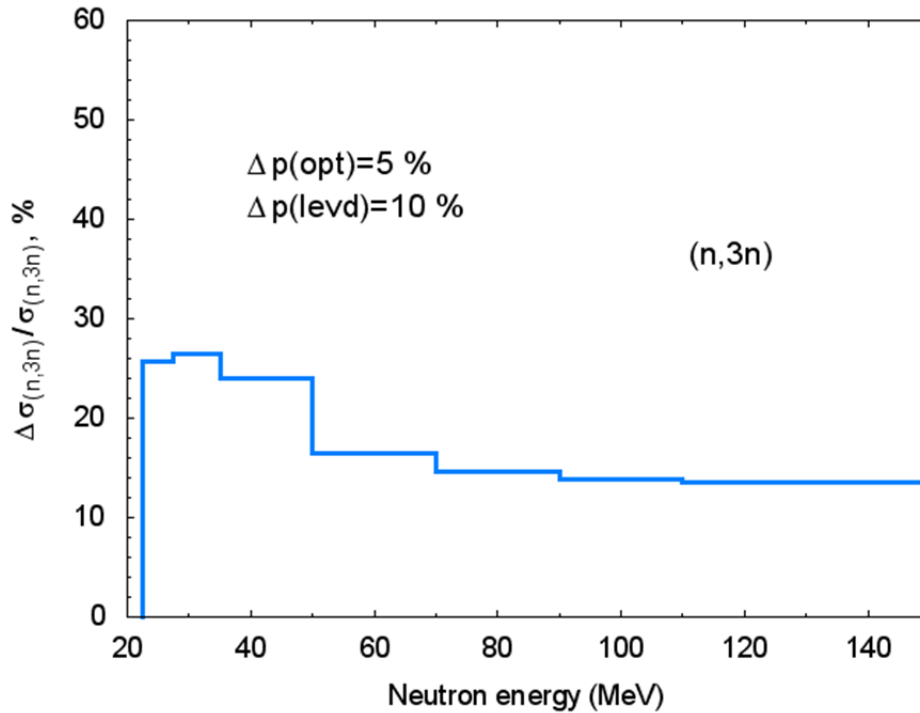


Fig.E13 The calculated RSD values of (n,3n) reaction cross-section for tungsten obtained with the variation of optical model and nuclear level density parameters with the RSD values equal to 5% and 10%, correspondingly.

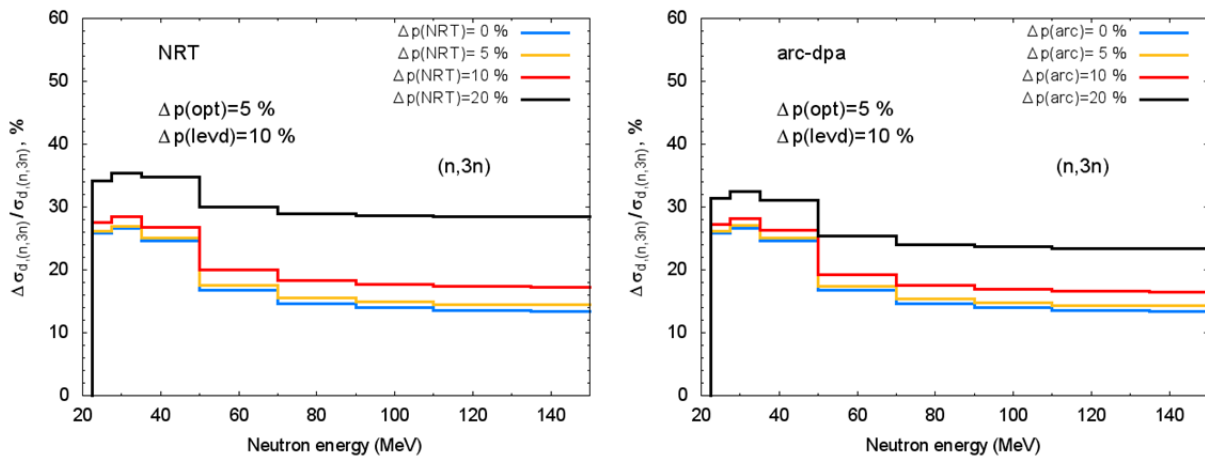


Fig.E14 The RSD values of (n,3n) reaction component of displacement cross-section for tungsten calculated using the NRT model (left) and the arc-dpa approach (right) with different variation of NRT and arc-dpa parameters, and the variation of optical model and nuclear level density parameters with the RSD values equal to 5% and 10%, correspondingly.

KIT Scientific Working Papers
ISSN 2194-1629

www.kit.edu